J. Fluid Mech. (1989), *vol.* 207, *pp.* 29–72
Printed in Great Britain

The motion of a rigid body in viscous fluid bounded by a plane wall

By RICHARD HSU† AND PETER GANATOS
Department of Mechanical Engineering, The City College of The City University of New York, New York, NY 10031, USA

(Received 9 January 1987 and in revised form 27 January 1989)

The boundary-integral method is used to calculate the hydrodynamic force and torque on an arbitrary body of revolution whose axis of symmetry is oriented at an arbitrary angle relative to a planar wall in the zero-Reynolds-number limit. The singular solution of the Stokes equations in the presence of a planar wall is used to formulate the integral equations, which are then reduced to a system of linear algebraic equations by satisfying the no-slip boundary conditions on the body surface using the boundary collocation method or weighted residual technique.

Numerical tests for the special case of a sphere moving parallel or perpendicular to a planar wall show that the present theory is accurate to at least three significant figures when compared with the exact solutions for gap widths as small as only one-tenth of the particle radius. Higher accuracy can be achieved and solutions can be obtained for smaller gap widths at the expense of more computation time and larger storage requirements.

The hydrodynamic force and torque on a spheroid with varying aspect ratio and orientation angle relative to the planar wall are obtained. The theory is also applied to study the motion of a toroidal particle or biconcave shaped disc adjacent to a planar wall. The coincidence of the drag and torque of a biconcave-shaped body and a torus having an aspect ratio $b/a = 2$ with the same surface area shows that in this case the hole of a torus has little influence on the flow field. On the other hand, for an aspect ratio $b/a = 10$, the effect of the hole is significant. It is also shown that when the body is not very close to the wall, an oblate spheroid can be used as a good approximation of a biconcave-shaped disc.

1. Introduction

The motion of an arbitrarily shaped rigid body in Stokes flow adjacent to a confining boundary has important biological and engineering applications. The theory may be used to model the flow of red blood cells in an artery or vein, see Wang & Skalak (1969), Chen & Skalak (1970), Leichtberg, Weinbaum & Pfeffer (1976). Specifically, the theory may explain the enhancement in the flux of oxygen and blood platelets near the artery wall resulting from the tumbling motion of the red blood cells, see Lightfoot (1974, p. 314). Other biological applications include the transport of non-spherical macromolecules or solute particles in intercellular clefts or through porous membranes. In particular, Brenner & Gaydos (1977) have shown how the hydrodynamic resistance coefficients describing the motion of non-spherical particles in the proximity of boundaries can be used in the study of diffusive and convective

† Current address: Department of Physiology, University of Arizona, Tucson, AZ 85724, USA.

transport of non-spherical solute particles. Other engineering applications include determination of the motion of a particle passing through an electrostatic precipitator or the trajectory of a contaminant particle in a lubricating bearing or in the laminar sublayer in the vicinity of a turbine blade.

A review of the low-Reynolds-number flow literature for the motion of a non-spherical particle in the presence of confining boundaries shows that, to date, five different methods of solution have been used to solve such problems. They are the method of reflections, the boundary collocation truncated series solution technique (multipole technique), the finite-element method, the singularity method and the boundary-integral method.

The method of reflections has been used extensively to study particle–particle and particle–boundary hydrodynamic interactions at low Reynolds number. This iterative solution technique, which in the present application alternately satisfies the no-slip boundary conditions on the particle surface and on the confining boundary, gives accurate results using one or two reflected fields only if the particle is far removed from the boundary. Using this approach, Wakiya (1959) treated the problem of the motion of a spheroidal particle parallel to a plane wall with the semi-major axis oriented at an arbitrary angle relative to the wall. This approximate solution will be used as a check of the more exact theory to be developed in the present paper, for the special case where the particle is a spheroid, in the limit as the spacing between the particle and the wall becomes large.

The boundary collocation, truncated series solution technique has been used to treat a wide variety of bounded and unbounded multiparticle Stokes flow problems. In connection with bounded flows involving non-spherical particles, the technique was used by Chen & Skalak (1970) to treat the problem of axisymmetric flow past a periodic array of spheroidal particles located at the centreline of an infinitely long circular cylinder. More recently, Kucaba-Pietal (1986) has used this technique to treat a torus in the vicinity of a planar wall for the special orientation where the axis of symmetry lies perpendicular to the wall. The method is capable of producing highly accurate results since each particle and boundary is represented by an infinite series or integral of all the simply separable solutions in the appropriate coordinate system, and the no-slip boundary conditions on all the surfaces are satisfied simultaneously rather than in an iterative fashion. However, in the present application involving a non-spherical particle inclined at an arbitrary angle relative to a planar wall, the coordinate transformation between the particle and boundary coordinate systems is complicated by the fact that the orientation angle of the particle enters as a parameter. This in turn complicates the inversion integrals which must be performed along the planar surface and requires that they be performed numerically which is exceedingly time consuming.

The finite-element method was used by Skalak, Chen & Chien (1972) in treating the problem of capillary blood flow consisting of biconcave disc-shaped solid particles periodically distributed along the axis of circular cylinder. The method permits one to treat body shapes that do no conform to a natural orthogonal coordinate system. However, it is computationally inefficient to use this method in Stokes flow problems where the fluid domain is not periodic and is of infinite extent as in the present case, since a large number of nodal points would be needed to describe the three-dimensional flow domain in which the slowly decaying particle disturbances are felt.

The singularity method is based on the principle of placing an appropriate set of singularities in the interior of each body in the flow field and satisfying the no-slip boundary conditions on the surface of each body, at least approximately. The

method has been used to treat slender bodies in the presence of confining boundaries, see Liron & Mochon (1976), Liron (1978). More recently, Dabros (1985) applied this method to calculate the angular velocity of a prolate spheroid adjacent to a planar wall and Yuan & Wu (1987) have used it to treat an arbitrary prolate body of revolution translating axisymmetrically towards a planar wall.

Odqvist (1930) developed a general solution of the Stokes equations, which allows the flow field to be expressed in terms of an integral over the boundary area of a Green function, which is the fundamental solution of the Stokes equations for a point force (stokeslet) multiplied by an unknown density function in each direction which represents the stress on the boundary surface. The density functions are determined by solving the integral equations that are obtained when the no-slip boundary conditions are applied on the boundary.

Youngren & Acrivos (1975) were the first investigators to use Odqvist's solution to calculate the creeping motion of an unbounded fluid past an arbitrary isolated three-dimensional body. The flow disturbance produced by the body was formulated as a system of linear integral equations for a distribution of stokeslets over the particle surface. The body surface was divided into a finite number of discrete elements in each of which the stokeslet strength was assumed to be constant, and the no-slip boundary conditions were applied at the centre of each element using a boundary collocation technique. Thus the integral equations were reduced to a system of linear algebraic equations for the unknown stokeslet densities. Later, Lewellen (1982) used a variation of this method to obtain a solution for the creeping motion of a spherical particle in an infinitely long cylindrical tube. The densities of the stokeslets were represented by a double infinite series, in contrast to discretizing the density functions as was done by Youngren & Acrivos (1975). The no-slip boundary conditions on the particle and boundary surfaces were satisfied by a weighted residual method in which the coefficients of the series representation were determined by requiring orthogonality of the residual vector to a set of trial functions. This approach of expressing the unknown surface stresses in terms of an infinite series eliminates the discretization error incurred if the integral equations were to be solved numerically by discretizing the force distribution to patches and will be used in the present study. More recently, Tozeren (1984) used the boundary integral technique to treat the problem of axisymmetric creeping flow past a collection of spheroids at the centreline of an infinitely long circular cylinder. A singularity solution in the presence of an infinitely long cylindrical surface for axisymmetric configurations was obtained and applied to formulate the integral equations. Thus the integrals along the infinite cylindrical surface vanish. The integral equations were solved numerically by discretizing the force distribution and using boundary collocation on the surface of the particles as was done by Youngren & Acrivos (1975). The advantage of utilizing a kernel function which identically satisfies the no-slip boundary conditions along the infinite boundary *a priori* is that it eliminates the need to perform time-consuming numerical integration along the boundary. This feature will be employed in the present work. From the above discussion, it appears that the boundary-integral technique is the best suited method for treating the present problem in terms of accuracy, ease of application and computational effort.

This paper is presented in six sections. In §2 the boundary-integral technique is used to formulate the problem for the hydrodynamic interaction of an arbitrarily shaped rigid body near a planar wall at low Reynolds number. This general solution is specialized to treat the very important case of an arbitrary body of revolution inclined at an arbitrary angle near a planar wall. In §3, the first highly accurate

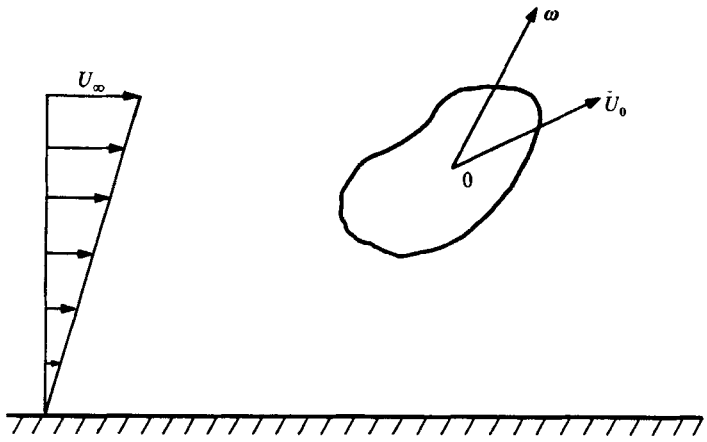

FIGURE 1. Motion of an arbitrarily shaped body in shear flow adjacent to a planar wall.

solutions for the force and torque on an oblate or prolate spheroidal particle near a planar wall are presented. In §4 the theory developed in §2 for treating an arbitrary body of revolution is modified to handle body shapes whose surface is a multivalued function of the axial coordinate and the first solutions for the force and torque on an arbitrarily inclined torus near a planar boundary are presented. In §5 the theory is applied to obtain the first solutions for a biconcave-shaped disc (shape of an undeformed red blood cell) next to a plane wall. Finally, §6 contains some concluding remarks about the applicability of the method in future research.

2. Formulation

The creeping motion of an arbitrary particle in an incompressible viscous fluid near an infinite planar wall is illustrated in figure 1. The particle has a translational velocity U_0 and is rotating with an angular velocity ω. U_∞ represents an undisturbed simple shear flow.

Let V_1 represent the flow field and define $V = V_1 - U_\infty$. The governing equations for V are

$$\mu \nabla^2 V = \nabla p, \quad \nabla \cdot V = 0, \tag{2.1a, b}$$

subject to the following boundary conditions:

at the particle surface
$$V = U_p \equiv U_0 + \omega \times \rho - U_\infty, \tag{2.2}$$

at the wall
$$V = 0, \tag{2.3}$$

at infinity
$$V = 0, \quad p = 0, \tag{2.4}$$

where ρ is the position vector whose origin is at the particle centre. In omitting the unsteady term from (2.1a) we have assumed that the particle is translating and rotating slowly enough such that the timescale to establish equilibrium in the fluid is much smaller than the time required for the particle surface to move a significant distance.

The boundary-value problem posed by (2.1)–(2.4) will be solved using the boundary-integral technique. We now outline the solution procedure.

As mentioned in the introduction, to avoid numerical integration over the infinite domain of the planar boundary, the singular solution for Stokes flow due to a point

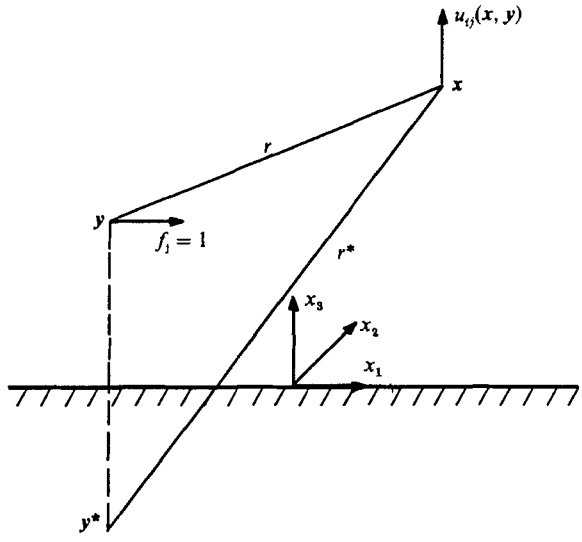

FIGURE 2. The flow field produced by a stokeslet in the vicinity of a planar wall.

force located near a stationary planar wall is used. Consider a semi-infinite fluid domain bounded by a planar wall as shown in figure 2. Let a unit singular force (stokeslet) pointing in the jth direction be located at a position (y_1, y_2, y_3). The velocity components and the associated pressure field at an arbitrary point (x_1, x_2, x_3) due to this stokeslet are given by Blake (1971) as

$$\left.\begin{aligned} u_{ij}(\boldsymbol{x},\boldsymbol{y}) &= \frac{1}{8\pi\mu}\left\{\left(\frac{1}{r}-\frac{1}{r^*}\right)\delta_{ij}+\frac{r_i r_j}{r^3}-\frac{r_i^* r_j^*}{r^{*3}}\right. \\ &\qquad \left. +2y_3(\delta_{j\alpha}\delta_{\alpha l}-\delta_{j3}\delta_{3l})\frac{\partial}{\partial r_l^*}\left(\frac{y_3 r_i^*}{r^{*3}}-\frac{\delta_{i3}}{r^*}-\frac{r_i^* r_3^*}{r^{*3}}\right)\right\}, \\ p_j(\boldsymbol{x},\boldsymbol{y}) &= \frac{1}{4\pi}\left\{\frac{r_j}{r^3}-\frac{r_j^*}{r^{*3}}-2y_3(\delta_{j\alpha}\delta_{\alpha l}-\delta_{j3}\delta_{3l})\frac{\partial}{\partial r_l^*}\left(\frac{r_j^*}{r^{*3}}\right)\right\}, \end{aligned}\right\} \tag{2.5}$$

where

$$r = [(x_1-y_1)^2+(x_2-y_2)^2+(x_3-y_3)^2]^{\frac{1}{2}},$$
$$r^* = [(x_1-y_1)^2+(x_2-y_2)^2+(x_3+y_3)^2]^{\frac{1}{2}};$$

$i, j, l = 1, 2, 3$; $\alpha = 1, 2$, and the usual summation convention is used. The term $\delta_{j\alpha}\delta_{\alpha l}-\delta_{j3}\delta_{3l}$ is not zero only when $j = l$, and has the value $+1$ for $j = 1$ or 2 and the value -1 for $j = 3$. The terms in (2.5) which involve r^* account for the disturbance of the wall in the flow field.

Using the notation of Youngren & Acrivos (1975), the Green's formula which may be applied to the Stokes problem is given by Ladyzhenskaya (1963, p. 53) as

$$\iiint_{\Omega}\left\{v_i\left[\mu\nabla^2 u_i-\frac{\partial q}{\partial x_i}\right]-u_i\left[\mu\nabla^2 v_i-\frac{\partial p}{\partial x_i}\right]\right\}\mathrm{d}\boldsymbol{x} = \iint_S \{v_i T_{ij}(\boldsymbol{u})\, n_j - u_i T_{ij}(\boldsymbol{v})\, n_j\}\,\mathrm{d}S. \tag{2.6}$$

The above formula is a general vector identity, where $\boldsymbol{u}$ and $\boldsymbol{v}$ are arbitrary smooth solenoidal vectors, p and q are arbitrary smooth scalar quantities, Ω represents a

bounded domain with boundary S, $\boldsymbol{n}$ is the outward pointing (with respect to Ω) normal on S and

$$\left.\begin{aligned} T_{ij}[\boldsymbol{u}] &= -\delta_{ij}\, q + \mu\left(\frac{\partial u_i}{\partial x_j} + \frac{\partial u_j}{\partial x_i}\right), \\ T_{ij}[\boldsymbol{v}] &= -\delta_{ij}\, p + \mu\left(\frac{\partial v_i}{\partial x_j} + \frac{\partial v_j}{\partial x_i}\right). \end{aligned}\right\} \tag{2.7}$$

Here $T_{ij}[\boldsymbol{v}]$ represents the local stress tensor corresponding to a flow field $(\boldsymbol{v}, p)$, and μ is the dynamic viscosity.

Replacing $(\boldsymbol{u}, q)$ in (2.6) with the singular solution $(u_{ij}(\boldsymbol{x}, \boldsymbol{y}), p(\boldsymbol{x}, \boldsymbol{y}))$ given by (2.5), and identifying $(\boldsymbol{v}, p)$ with the solution of the boundary-value problem posed by (2.1)–(2.4), we get

$$v_i(\boldsymbol{y}) = \iint_{S_p} \{-T_{kj}[\boldsymbol{u}^i(\boldsymbol{x}, \boldsymbol{y})]\, v_k(\boldsymbol{x})\, n_j(\boldsymbol{x}) + T_{kj}[\boldsymbol{v}(\boldsymbol{x})]\, n_j(\boldsymbol{x})\, u_{ki}(\boldsymbol{x}, \boldsymbol{y})\}\, \mathrm{d}S_x \tag{2.8}$$

Here $\boldsymbol{u}^i(\boldsymbol{x}, \boldsymbol{y})$ represents the velocity field due to a stokeslet pointing in the ith direction, $\mathrm{d}S_x$ indicates that the integration is performed with respect to the variable $\boldsymbol{x}$, S_p represents the surface of the particle, and $\boldsymbol{n}$ is the inward normal to the object. The corresponding pressure is obtained from (2.1) using (2.8). The solution can be written as

$$\left.\begin{aligned} \boldsymbol{v}_i(\boldsymbol{y}) &= v_i^{(1)}(\boldsymbol{y}) + v_i^{(2)}(\boldsymbol{y}), \\ p(\boldsymbol{y}) &= p^{(1)}(\boldsymbol{y}) + p^{(2)}(\boldsymbol{y}), \end{aligned}\right\} \tag{2.9}$$

where

$$\begin{aligned} v_i^{(1)}(\boldsymbol{y}) &= \iint_{S_p} u_{ki}(\boldsymbol{x}, \boldsymbol{y})\, T_{kj}[\boldsymbol{v}(\boldsymbol{x})]\, n_j\, \mathrm{d}S_x \\ &= \iint_{S_p} u_{ki}(\boldsymbol{x}, \boldsymbol{y}) f_k(\boldsymbol{x})\, \mathrm{d}S_x \\ &= \frac{1}{8\pi\mu} \iint_{S_p} \left\{\left(\frac{1}{r} - \frac{1}{r^*}\right)\delta_{ik} + \left(\frac{r_i r_k}{r^3} - \frac{r_i^* r_k^*}{r^{*3}}\right)\right. \\ &\quad \left. + 2y_3(\delta_{i\alpha}\delta_{\alpha l} - \delta_{i3}\delta_{3l}) \frac{\partial}{\partial r_l^*}\left(\frac{y_3 r_k^*}{r^{*3}} - \frac{\delta_{k3}}{r^*} - \frac{r_3^* r_k^*}{r^{*3}}\right)\right\} f_k(\boldsymbol{x})\, \mathrm{d}S_x, \end{aligned} \tag{2.10}$$

$$\begin{aligned} v_i^{(2)}(\boldsymbol{y}) &= -\iint_{S_p} T_{kj}[\boldsymbol{u}^i(\boldsymbol{x}, \boldsymbol{y})]\, v_k(\boldsymbol{x})\, n_j(\boldsymbol{x})\, \mathrm{d}S_x \\ &= \frac{3}{4\pi} \iint_{S_p} \frac{r_i r_j r_k}{r^5} - \frac{r_i^* r_j^* r_k^*}{r^{*5}} - 2y_3(\delta_{i\alpha}\delta_{\alpha l} - \delta_{i3}\delta_{3l}) \\ &\quad \times \frac{\partial}{\partial r_l^*}\left(\frac{r_3^* r_j^* r_k^*}{r^{*5}} - \frac{r_j^* r_k^* y_3}{r^{*5}} + \frac{y_3}{r^{*3}}\delta_{jk}\right) v_k(\boldsymbol{x})\, n_j(\boldsymbol{x})\, \mathrm{d}S_x, \end{aligned} \tag{2.11}$$

$$p^{(1)}(\boldsymbol{y}) = \frac{1}{4\pi} \iint_{S_p} \left\{\frac{r_k}{r^3} - \frac{r_k^*}{r^{*3}} - 2y_3(\delta_{kl}\delta_{l3} - \delta_{k3}\delta_{3l}) \frac{\partial}{\partial r_l^*}\left(\frac{r_3^*}{r^{*3}}\right)\right\} f_k(\boldsymbol{x})\, \mathrm{d}S_x, \tag{2.12}$$

$$\begin{aligned} p^{(2)}(\boldsymbol{y}) &= \frac{1}{2\pi} \iint_{S_p} \left\{\left(\frac{1}{r^3} - \frac{1}{r^{*3}}\right)\delta_{kj} - 3\left(\frac{r_k r_j}{r^5} - \frac{r_k^* r_j^*}{r^{*5}}\right)\right. \\ &\quad + (\delta_{j\alpha}\delta_{\alpha l} - \delta_{j3}\delta_{3l}) \frac{\partial}{\partial r_l^*}\left(\frac{x_3}{r^{*3}}\delta_{k3} + \frac{3r_k r_j y_3}{r^{*5}}\right) \\ &\quad \left. + (\delta_{k\alpha}\delta_{\alpha l} - \delta_{k3}\delta_{3l}) \frac{\partial}{\partial r_l^*}\left(\frac{x_3}{r^{*3}}\delta_{j3} - \frac{3r_k r_j y_3}{r^{*5}}\right)\right\} v_k(\boldsymbol{x})\, n_j(\boldsymbol{x})\, \mathrm{d}S_x \end{aligned} \tag{2.13}$$

The quantities $(v_i^{(1)}, p^{(1)})$ and $(v_i^{(2)}, p^{(2)})$ have traditionally been called single- and double-layer potentials having densities f_k and v_k respectively. The quantity $f_k = T_{kj} n_j$ is the density of the stokeslets, identical to the local surface stress force in the kth direction.

The solution for v_i and p, given by (2.9), satisfies the governing equations (2.1), the no-slip boundary conditions on the infinite wall and tends zero at infinity. Therefore it only remains to satisfy the no-slip boundary conditions on the surface of the particle.

In the above formulae it has been assumed that the particle boundary S_p is a Lyapunov surface, i.e. that the surface has a well-defined tangent plane at every point. Under this assumption, the single-layer potential $v_i^{(1)}$ is continuous in the fluid domain Ω and at the particle surface S_p. However, it is well known that the double-layer potential $v_i^{(2)}$ undergoes a discontinuity at S_p given by

$$\lim_{y \to y_0} v_i^{(2)}(y) = v_i^{(2)}(y_0) + \tfrac{1}{2} v_i(y_0), \quad y \in \Omega, \quad y_0 \in S_p. \tag{2.14}$$

Therefore using (2.14) and applying the no-slip boundary conditions on the surface of the particle leads to the following linear integral equations to be solved for the unknown density functions f_k:

$$\begin{aligned} v_i(y) = \frac{1}{4\pi\mu} \iint_{S_p} \Bigg\{ & \left(\frac{1}{r} - \frac{1}{r^*}\right) \delta_{ik} + \frac{r_i r_k}{r^3} - \frac{r_i^* r_k^*}{r^{*3}} \\ & + 2y_3 (\delta_{i\alpha} \delta_{\alpha l} - \delta_{i3} \delta_{3l}) \left(\frac{3x_3 r_i^* r_k^*}{r^{*5}} - \frac{x_3}{r^{*3}} \delta_{ik} + \frac{r_i^*}{r^{*3}} \delta_{k3} \right. \\ & \left. - \frac{r_k^*}{r^{*3}} \delta_{i3} \right) \Bigg\} f_k(x) \, dS_x + \frac{3}{2\pi} \iint_{S_p} \Bigg\{ \frac{r_i r_j r_k}{r^5} \\ & - \frac{r_i^* r_j^* r_k^*}{r^5} - 2y_3 (\delta_{i\alpha} \delta_{\alpha l} - \delta_{i3} \delta_{3l}) \left(\frac{-5x_3 r_i^* r_j^* r_k^*}{r^{*7}} \right. \\ & \left. + \frac{r_j^* r_k^*}{r^{*5}} \delta_{i3} + \frac{x_3 r_j^*}{r^{*5}} \delta_{ik} + \frac{x_3 r_k^*}{r^{*5}} \delta_{ij} - \frac{y_3 r_i^*}{r^{*5}} \delta_{jk} \right) \Bigg\} \\ & \times v_k(x) \, n_j(x) \, dS_x, \quad y \in S_p. \end{aligned} \tag{2.15}$$

The solution of the velocity and pressure fields (2.9) with the density distribution given by (2.15) is valid for any steady motion of a particle of arbitrary shape adjacent to a planar wall at low Reynolds number. The system of integral equations (2.15) can only be solved numerically. This requires discretization of the unknown density functions and double numerical integration over the surface of the particle. An important special case of problems may be solved much more accurately and efficiently by considering only bodies of revolution with the motion having planar symmetry.

In this special case a cylindrical coordinate system (R, θ, Z) is used, as shown in figure 3. The Z-axis lies along the particle axis of symmetry and the radius of the body surface, R, can be represented by a single-valued function

$$R = R_S(Z). \tag{2.16}$$

The transformation of coordinates (R, θ, Z) to (x_1, x_2, x_3) is given by

$$\left.\begin{aligned} x_1 &= Z \cos\alpha - R \sin\alpha \cos\theta, \\ x_2 &= -R \sin\theta, \\ x_3 &= Z \cos\alpha + R \cos\alpha \cos\theta + H, \end{aligned}\right\} \tag{2.17}$$

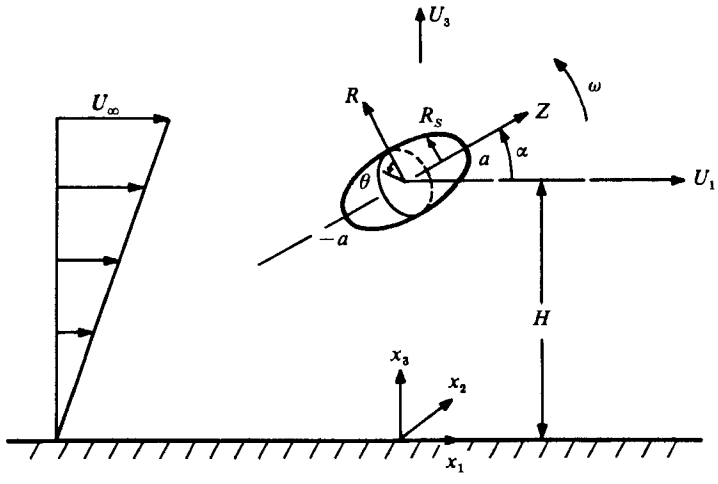

FIGURE 3. The planar motion of a body of revolution in shear flow near a planar wall.

where α is the orientation angle of the body and H is the perpendicular distance from the centre of the body to the wall as shown in figure 3. Using (2.16) and (2.17) and denoting the coordinates of the points $\boldsymbol{x}$ and $\boldsymbol{y}$ by $(R_S(Z), \theta, Z)$ and $(R_S(Z^*), \theta^*, Z^*)$ in the cylindrical coordinate system respectively, all variables in (2.15) can be expressed as functions of θ, θ^*, Z and Z^*. The unknown density functions for the motion having planar symmetry can be represented by the Fourier–Legendre series

$$\left.\begin{aligned} f_1 &= \sum_{m=0}^{\infty}\sum_{n=0}^{\infty} A_{1,m,n} P_n\left(\frac{Z}{a}\right)\cos m\theta, \\ f_2 &= \sum_{m=1}^{\infty}\sum_{n=0}^{\infty} A_{2,m,n} P_n\left(\frac{Z}{a}\right)\sin m\theta, \\ f_3 &= \sum_{m=0}^{\infty}\sum_{n=0}^{\infty} A_{3,m,n} P_n\left(\frac{Z}{a}\right)\cos m\theta, \end{aligned}\right\} \tag{2.18}$$

where P_n is the Legendre function of order n, and $A_{k,m,n}$ are coefficients to be determined.

To solve the integral equation (2.15) we define a residual vector $v_i^{\mathrm{R}}(\boldsymbol{y})$ as follows:

$$v_i^{\mathrm{R}}(\boldsymbol{y}) = v_i(\boldsymbol{y}) - v_i^*(\boldsymbol{y}), \tag{2.19}$$

where $v_i(\boldsymbol{y})$ represents the true solution and $v_i^*(\boldsymbol{y})$ is the right-hand side of the integral equation (2.15). If the stokeslet density function $f_k(\boldsymbol{x})$ in (2.15) is exact, the residual vector $v_i^{\mathrm{R}}(\boldsymbol{y})$ will be identically zero. To find an approximate solution of $f_k(\boldsymbol{x})$ we shall use two different methods.

(*a*) The boundary-collocation method: In this method we let the residual vector $v_i^{\mathrm{R}}(\boldsymbol{y})$ vanish at discrete points on the surface of the body. Substituting the series representations for f_k into (2.15), truncating the series for f_k after M terms in m and N terms in n and choosing $M \times N$ collocation points on the surface of the particle on which the no-slip boundary conditions are satisfied, leads to $3 \times M \times N$ linear algebraic equations for the $3 \times M \times N$ unknown $A_{k,m,n}$ coefficients. The integrals in (2.15) are performed analytically in the θ-direction and numerically in the Z-direction. The evaluation of the integrals in the θ-direction is outlined in Appendix A. A copy of the

final expressions of the double integrals in (2.15) in terms of integrations only in the Z-direction may be obtained from the authors on request.

(*b*) Weighted residual method: In this method we multiply the residual vector by trial functions $F_i(\theta^*, Z^*)$, which are equal to $\cos m\theta^* P_n(Z^*/a)$ for $i = 1$ or 3 and $\sin m\theta^* P_n(Z^*/a)$ for $i = 2$, and let the weighted residual vanish, i.e.

$$\int_{-a}^{+a}\int_{0}^{2\pi} V_i^{\mathrm{R}}(R_S(Z^*),\, \theta^*,\, Z^*)\, F_i(\theta^*,\, Z^*)\, R_S(Z^*)\left[1+\left(\frac{\mathrm{d}R_S}{\mathrm{d}Z^*}\right)^2\right]^{\frac{1}{2}} \mathrm{d}\theta^*\,\mathrm{d}Z^* = 0. \quad (2.20)$$

Taking $n = 0, 1, 2, \ldots, N-1$, $m = 0, 1, 2, \ldots, M-1$ for $i = 1$ and 3 and $m = 1, 2, 3, \ldots, M$ for $i = 2$, we also get $3 \times M \times N$ linear algebraic equations for the $3 \times M \times N$ unknown coefficients $A_{k,m,n}$. The integration in the θ- and Z-directions for calculating v_i^{R} is performed in the same way as in the boundary-collocation method, while the outer integration in the θ^*- and Z^*-directions is performed using a composite 8-point Gaussian–Legendre quadrature formula.

After the $A_{k,m,n}$ coefficients are obtained by either method, the total force and torque acting on the particle may be computed from

$$F_k = 2\pi \sum_{n=0}^{N-1}\left\{A_{k,0,n}\int_{-a}^{+a} P_n\left(\frac{Z}{a}\right) R_S(Z)\left[1+\left(\frac{\mathrm{d}R_S}{\mathrm{d}Z}\right)^2\right]^{\frac{1}{2}}\mathrm{d}Z\right\} \quad (k = 1 \text{ and } 3), \quad (2.21)$$

$$\begin{aligned} T_2 = \pi \sum_{n=0}^{N-1}\Bigg\{ & 2(A_{1,0,n}\sin\alpha - A_{3,0,n}\cos\alpha)\int_{-a}^{+a} Z R_S(Z) \\ & \times\left[1+\left(\frac{\mathrm{d}R_S}{\mathrm{d}Z}\right)^2\right]^{\frac{1}{2}}\mathrm{d}Z + (A_{1,1,n}\cos\alpha + A_{3,1,n}\sin\alpha) \\ & \times\int_{-a}^{+a} R_S^2(Z)\left[1+\left(\frac{\mathrm{d}R_S}{\mathrm{d}Z}\right)^2\right]^{\frac{1}{2}}\mathrm{d}Z\Bigg\}. \end{aligned} \quad (2.22)$$

The accuracy and convergence characteristics of the two methods is explored in Appendix B where detailed comparison is made with exact solutions for the hydrodynamic force and torque on a spherical particle near a planar wall.

3. Solutions for the motion of a spheroid near a planar wall

In this section the theory derived in §2 is used to obtain solutions for the motion of a spheroid near a planar wall. The surface of the body is represented in the cylindrical coordinate system (see figure 3) by

$$R_S(Z) = b\left[1-\left(\frac{Z}{a}\right)^2\right]^{\frac{1}{2}}, \quad (3.1)$$

where the spheroid is oblate for $a < b$ and prolate for $a > b$.

Let a spheroid translate with velocity components U_1 and U_3 in the directions parallel and perpendicular to the wall respectively, and rotate with angular velocity ω about the axis x_2. The undisturbed shear flow has a gradient S. The force and torque on the spheroid may be related to the particle velocity and shear strength using twelve dimensionless resistance coefficients as follows:

$$\begin{pmatrix} F_1 \\ F_3 \\ T_2 \end{pmatrix} = 6\pi\mu c \begin{pmatrix} F_1^{t_1} & F_1^{t_3} & F_1^{r} & HF_1^{S} \\ F_3^{t_1} & F_3^{t_3} & F_3^{r} & HF_3^{S} \\ \frac{4}{3}bT_2^{t_1} & \frac{4}{3}bT_2^{t_3} & \frac{4}{3}bT_2^{r} & \frac{2}{3}b^2T_2^{S} \end{pmatrix} \begin{pmatrix} U_1 \\ U_3 \\ b\omega \\ S \end{pmatrix}. \quad (3.2)$$

N	$F_3^{t_2}/F_{3,\infty}^{t_3}$	$F_1^{t_1}/F_{1,\infty}^{t_1}$	$T_2^{t_1}$	$T_2^{r}/T_{2,\infty}^{r}$	$F_1^{s}/F_{1,\infty}^{s}$	$T_2^{s}/T_{2,\infty}^{s}$
			$H/b = 0.55$			
2	8.9	4.732	−0.168	12.05	1.421	−1.23
4	23.7	3.218	0.475	4.47	1.991	1.36
6	40.3	3.355	0.580	5.19	1.985	1.32
8	53.1	3.374	0.588	4.90	1.994	1.43
10	57.5	3.378	0.576	4.80	1.990	1.31
12	60.4	3.381	0.567	5.12	1.984	1.28
14	61.4	3.384	0.561	4.90	1.988	1.34
16	61.7	3.386	0.557	4.80	1.990	1.41
18	62.6	3.388	0.556	4.91	1.992	1.43
20	62.9	3.389	0.555	5.03	1.990	1.37
22	62.9	3.389	0.555	5.04	1.988	1.36
24		3.390	0.555	5.03	1.988	1.35
26		3.390		4.97	1.988	1.35
			$H/b = 0.8$			
2	5.326	1.850	0.0134	0.843	1.516	0.780
4	6.918	1.917	0.1233	1.670	1.664	1.363
6	7.226	1.923	0.1217	1.656	1.671	1.370
8	7.257	1.923	0.1211	1.655	1.670	1.369
10	7.263	1.923	0.1211	1.654	1.670	1.369
12	7.264		0.1211	1.654		1.369
14	7.262					
16	7.262					
18	7.262					
			$H/b = 1.1$			
2	3.407	1.460	0.01057	0.672	1.354	0.915
4	3.567	1.564	0.05913	1.242	1.478	1.354
6	3.589	1.568	0.05921	1.245	1.481	1.362
8	3.589	1.568	0.05916	1.245	1.480	1.361
10	3.589	1.568	0.05916	1.245	1.480	1.361
			$H/b = 1.5$			
2	2.393	1.267	0.00647	0.625	1.230	0.955
4	2.379	1.376	0.03243	1.100	1.342	1.324
6	2.285	1.380	0.03251	1.102	1.346	1.331
8	2.385	1.380	0.03251	1.102	1.346	1.331

TABLE 1. Convergence of the resistance coefficients for an oblate spheroid having aspect ratio $a/b = 0.5$ with its symmetry axis oriented perpendicular to the wall

Here $c = b$ for an oblate spheroid and $c = a$ for a prolate spheroid, H is the distance between the centre of the spheroid and the wall, F_1 and F_3 are the force components in the x_1 and x_3 directions respectively and T_2 is the torque acting on the spheroid.

All the dimensionless resistance coefficients are functions of the separation distance of the spheroid from the wall, the orientation angle of the spheroid relative to the wall and the aspect ratio of the spheroid. The separation will be expressed by the dimensionless parameter H/c. The aspect ratio ϵ is defined as a/b for an oblate spheroid and b/a for a prolate spheroid, so that it varies between zero and unity in both cases.

It is worth noting that only nine of the twelve resistance coefficients are

	$a/b = 0.1$				$a/b = 0.5$			
M...	4	6	8	10	4	6	8	10
N				(*a*) $H/c = 1.1$				
4	2.50	2.53	2.55	2.57	4.80	5.02	5.21	5.21
6	2.51	2.59	2.61	2.61	4.96	5.08	5.16	5.16
8	2.53	2.71	2.72	2.72	5.03	5.15	5.20	5.20
10	2.54	2.71	2.72	2.72	5.04	5.15	5.20	5.20
				$H/c = 1.5$				
4	1.741	1.741	1.742		2.363	2.364	2:365	
6	1.833	1.837	1.838		2.368	2.370	2.370	
8	1.834	1.840	1.840		2.369	2.370	2.370	
10	1.835	1.840	1.840					
				(*b*) $H/c = 1.1$				
4	1.314	1.320	1.328	1.330	1.294	1.303	1.324	1.322
6	1.317	1.324	1.330	1.331	1.296	1.307	1.310	1.310
8	1.318	1.338	1.339	1.339	1.297	1.309	1.313	1.313
10	1.321	1.338	1.339	1.339	1.298	1.309	1.313	1.313
				$H/c = 1.5$				
4	1.081	1.081	1.081		1.070	1.070	1.071	
6	1.087	1.087	1.087		1.071	1.071	1.071	
8	1.087	1.087	1.087		1.071	1.071	1.071	
				(*c*) $H/c = 1.1$				
4	−0.187	−0.189	−0.192	−0.192	−0.193	−0.198	−0.202	−0.201
6	−0.187	−0.190	−0.192	−0.193	−0.193	−0.194	−0.195	−0.195
8	−0.189	−0.194	−0.194	−0.194	−0.193	−0.194	−0.195	−0.195
10	−0.190	−0.194	−0.194	−0.194	−0.193	−0.194	−0.195	−0.195
				$H/c = 1.5$				
4	−0.0660	−0.0660	−0.0660		−0.0591	−0.0591	−0.0591	
6	−0.0662	−0.0666	−0.0667		−0.0588	−0.0589	−0.0589	
8	−0.0663	−0.0667	−0.0667		−0.0588	−0.0589	−0.0589	

TABLE 2. Convergence tests of (*a*) $F_3^t/F_{3,\infty}^t$, (*b*) $T_2^r/T_{2,\infty}^r$ and (*c*) T_2^t for an oblate spheroid inclined at $\alpha = 15°$ relative to a planar wall. N = number of rings (constant values of Z), M = number of collocation points on each ring (constant values of θ)

independent. From reciprocity theorems, Brenner (1964), three pairs of the resistance coefficients are related as follows:

$$F_1^{t_3} = F_3^{t_1}, \tag{3.3}$$

$$F_1^r = \tfrac{4}{3}T_2^{t_1}, \tag{3.4}$$

$$F_3^r = \tfrac{4}{3}T_2^{t_3}. \tag{3.5}$$

These relations are used as a further check of the consistency of the numerical results.

Table 1 shows convergence tests of the force and torque coefficients for an oblate spheroid having aspect ratio $a/b = 0.5$ with its axis of symmetry oriented perpendicular to the wall (i.e. $\alpha = 90°$). For this particular case only one-dimensional collocation is required. Note that the convergence for $H/b = 0.55$, which is equivalent to $H/a = 1.1$, is somewhat slower than for a sphere with $H/a = 1.1$ (see Appendix B).

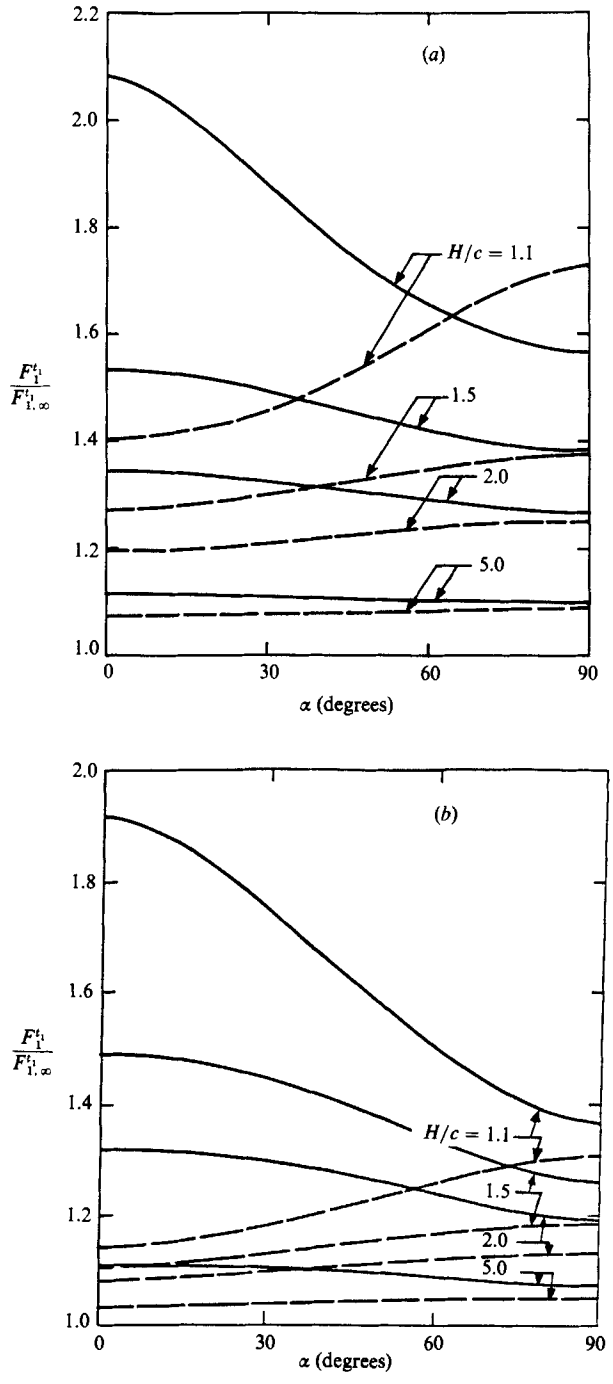

FIGURE 4. The drag force on an oblate or prolate spheroid having aspect ratio (*a*) $\epsilon = 0.5$, (*b*) $\epsilon = 0.1$, translating parallel to a wall. ——, oblate; – – –, prolate.

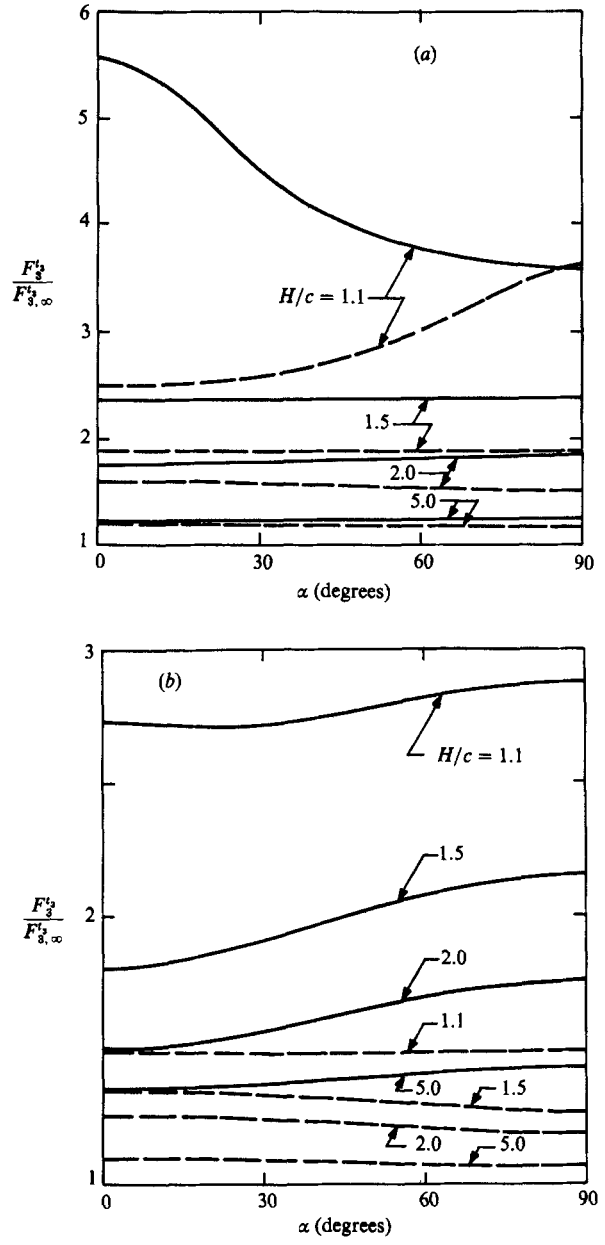

FIGURE 5. The drag force on an oblate or prolate spheroid having aspect ratio (*a*) $\epsilon = 0.5$, (*b*) $\epsilon = 0.1$, translating perpendicular to a wall. ——, oblate; – – –, prolate.

When the particle is oriented at an arbitrary angle relative to the wall two-dimensional collocation is required. The rate of convergence is found to be similar to the case of a sphere (see Appendix B) if we replace H/a by H/c. Table 2 shows the convergence of the coefficients $F_3^{t_3}$, T_2^{r} and $T_3^{t_3}$ for an oblate spheroid having aspect ratios $\epsilon = 0.1$ and 0.5 inclined at $\alpha = 15°$ relative to the wall. The remaining resistance coefficients exhibited similar convergence characteristics and are not shown. Inspection of this table shows that convergence to three or four significant

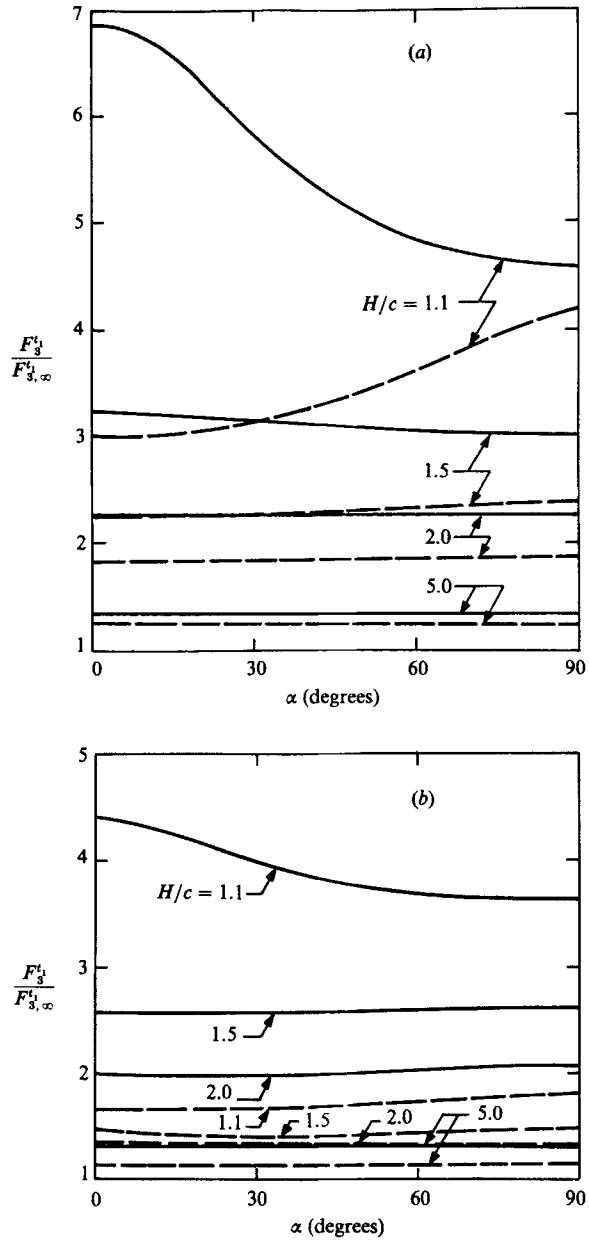

FIGURE 6. The force component perpendicular to the wall on an oblate or prolate spheroid having aspect ratio (*a*) $\epsilon = 0.5$, (*b*) $\epsilon = 0.1$, due to translation parallel to the wall. ——, oblate; – – –, prolate.

figures can be achieved for spacings H/c as close as 1.1 using a maximum of 10 rings with 10 points on each ring. Larger spacings ($H/c > 1.5$) require only 4–6 rings and points to achieve the same accuracy.

Figures 4–12 show the converged values of the dimensionless hydrodynamic force and torque coefficients for an oblate and prolate spheroid as a function of the orientation angle α for constant values of separation distance H/c and aspect ratio ϵ. The coefficients are presented as the ratios of their values in the presence of the wall

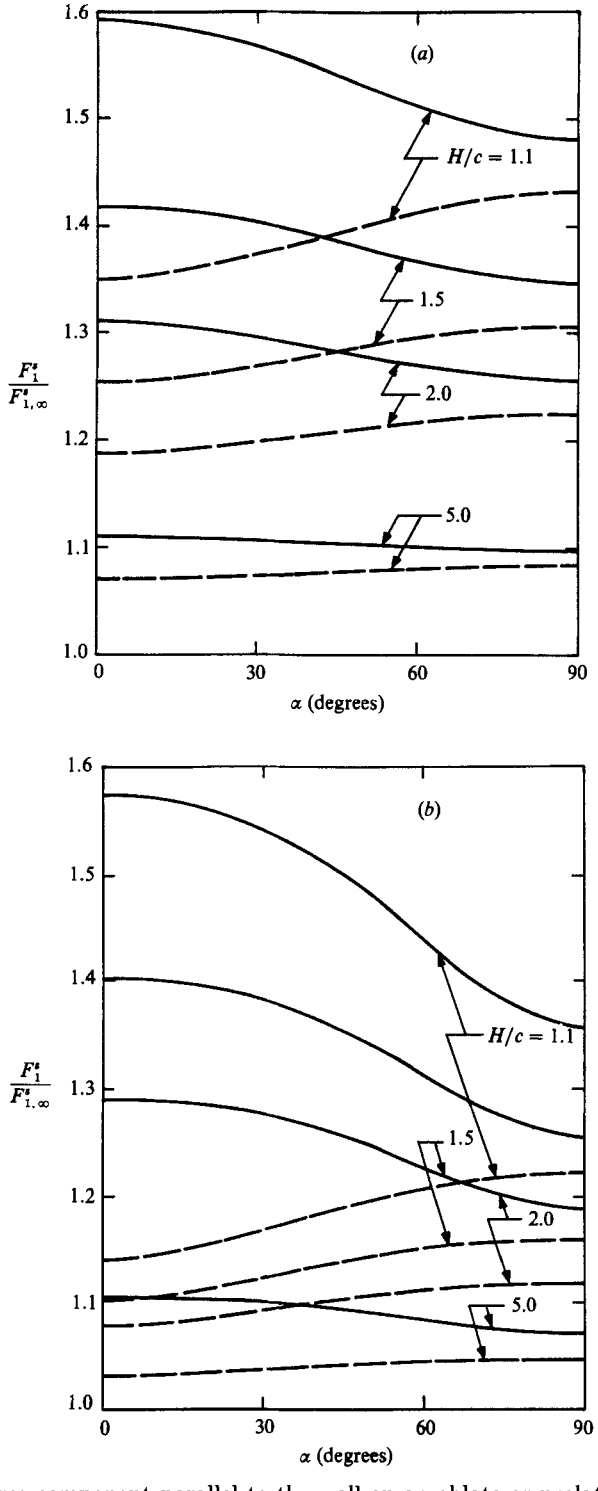

FIGURE 7. The force component parallel to the wall on an oblate or prolate spheroid having aspect ratio (*a*) $\epsilon = 0.5$, (*b*) $\epsilon = 0.1$, which is rigidly held in a shear flow. ——, oblate; – – –, prolate.

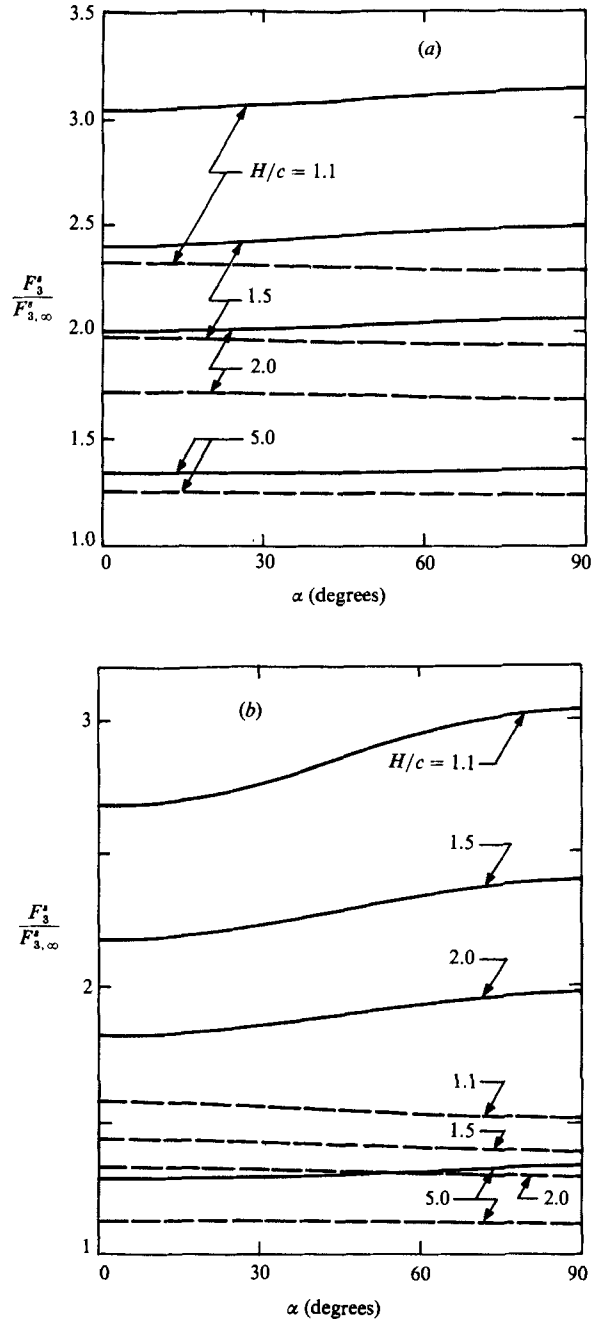

FIGURE 8. The force component perpendicular to the wall on an oblate or prolate spheroid having aspect ratio (*a*) $\epsilon = 0.5$, (*b*) $\epsilon = 0.1$, which is rigidly held in a shear flow. ——, oblate; – – –, prolate.

to the corresponding values in an unbounded fluid domain, except for the torque coefficients $T_2^{t_1}$ and $T_2^{t_3}$ for translation parallel and perpendicular to the wall which are identically zero in the absence of the wall. The hydrodynamic force coefficients of a spheroid moving parallel or perpendicular to its axis of symmetry in an unbounded fluid domain were obtained by Oberbeck and are presented by Happel & Brenner

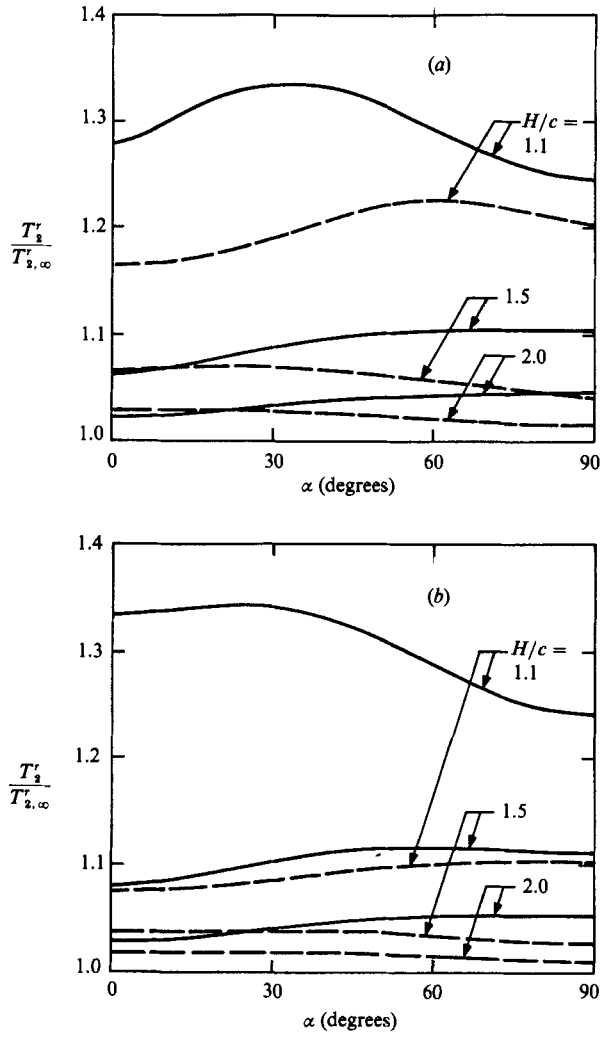

FIGURE 9. Torque on a rotating oblate or prolate spheroid having aspect ratio (*a*) $\epsilon = 0.5$, (*b*) $\epsilon = 0.1$ in the vicinity of a planar wall. ——, oblate; – – –, prolate.

(1973, p. 223). The torque coefficients of a spheroid which is rotating in an otherwise quiescent unbounded fluid or rigidly held in an unbounded shear flow $U_\infty = Sx_3$ were obtained by Jeffery (1922). A summary of these formulas is presented in Appendix C for reference.

Figures 4 and 5 show $F_1^{t_1}/F_{1,\infty}^{t_1}$ and $F_3^{t_3}/F_{1,\infty}^{t_3}$, the ratios of the drag force for the motion parallel and perpendicular to the wall, respectively, to the corresponding force when $H \to \infty$. The curves of $F_1^{t_1}/F_{1,\infty}^{t_1}$ are similar in shape for both $\epsilon = 0.5$ and 0.1 with the values for $\epsilon = 0.1$ somewhat smaller than for $\epsilon = 0.5$. However the behaviour of $F_3^{t_3}/F_{3,\infty}^{t_3}$ is radically different for $\epsilon = 0.1$ and 0.5, especially at close spacings. For an oblate spheroid at $H/b = 1.1$ the ratio $F_3^{t_3}/F_{3,\infty}^{t_3}$ decreases with increasing α for $\epsilon = 0.5$ while it increases for $\epsilon = 0.1$.

Figure 6 shows $F_3^{t_1}/F_{3,\infty}^{t_1}$, the ratio of the force component perpendicular to the wall due to the motion parallel to the wall to the same force in the absence of the wall. Although the values of $F_3^{t_1}$ are zero for the orientation angle α equal to 0° and 90°,

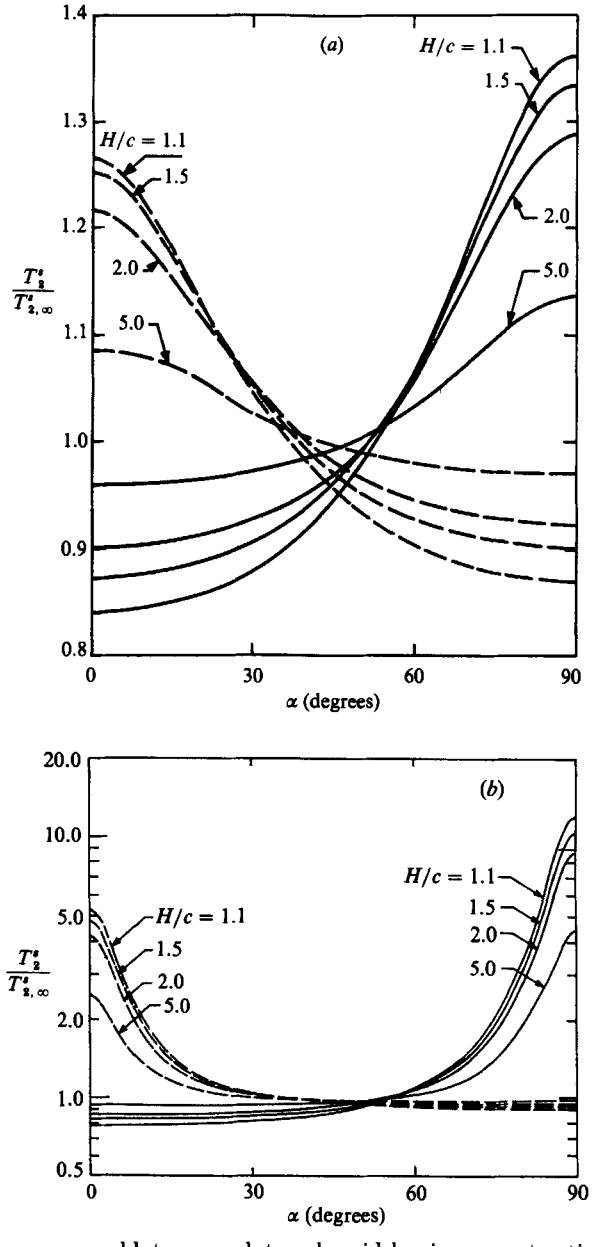

FIGURE 10. Torque on an oblate or prolate spheroid having aspect ratio (*a*) $\epsilon = 0.5$, (*b*) $\epsilon = 0.1$, which is rigidly held in a shear flow in the vicinity of a planar wall. ——, oblate; – – –, prolate.

the ratio $F_3^{t_1}/F_{3,\infty}^{t_1}$ has a finite limiting value for each particle-to-wall spacing at the two extreme points. The ratio $F_3^{t_1}/F_{3,\infty}^{t_1}$ is a weak function of α up to $H/c = 1.5$ but becomes strongly dependent on α when the spheroid is closer to the wall.

Figures 7 and 8 show the variation of ratios $F_1^s/F_{1,\infty}^s$ and $F_3^s/F_{3,\infty}^s$ respectively. It is interesting to note that $F_{1,\infty}^s = -F_{1,\infty}^{t_1}$ and $F_{3,\infty}^s = -F_{3,\infty}^{t_1}$. Comparing with figures 4 and 5, the absolute value of F_1^s is always less than $F_1^{t_1}$, and the absolute value of F_3^s is always less than $F_3^{t_1}$, and their difference increases as the particle is brought closer to the wall.

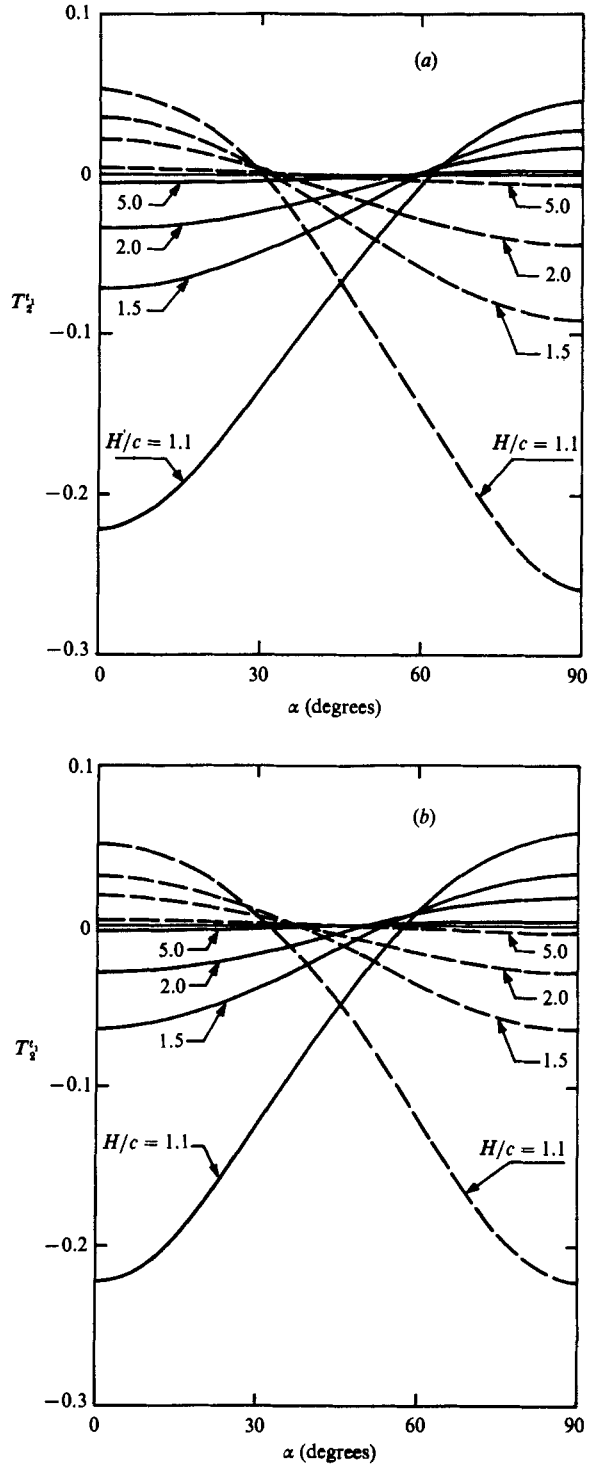

FIGURE 11. Torque on an oblate or prolate spheroid having aspect ratio (*a*) $\epsilon = 0.5$, (*b*) $\epsilon = 0.1$, due to translation parallel to the wall. ——, oblate; – – –, prolate.

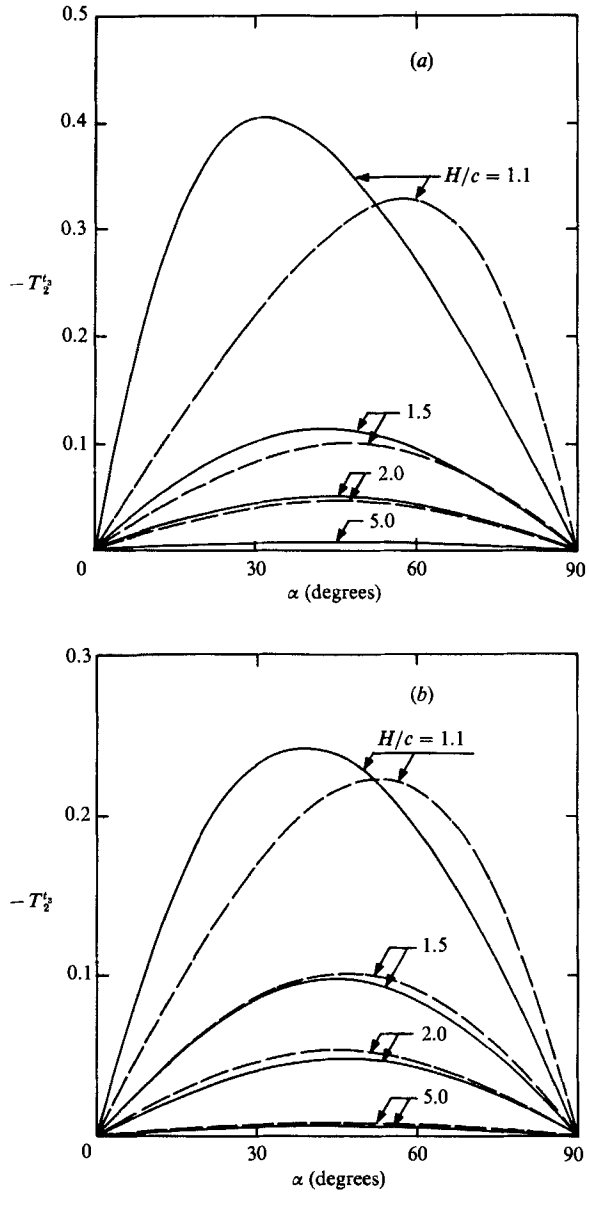

FIGURE 12. Torque on an oblate or prolate spheroid having aspect ratio (*a*) $\epsilon = 0.5$, (*b*) $\epsilon = 0.1$, due to translation perpendicular to the wall. ——, oblate; – – –, prolate.

Figure 9 shows $T_2^r/T_{2,\infty}^r$, the ratio of the torque experienced by a rotating spheroid to the value in an unbounded fluid domain. The ratio is almost unity for H/c greater than 5. When the separation distance is decreased, the orientation angle α at which $T_2^r/T_{2,\infty}^r$ becomes maximum gradually shifts from $\alpha = 0°$ toward 90° for an oblate spheroid and vice versa for a prolate spheroid.

All the ratios shown above are greater than unity for any orientation angle α, so these force and torque coefficients are always larger than the corresponding values in an unbounded fluid domain. However, for the ratio $T_2^s/T_{2,\infty}^s$ this is not the case,

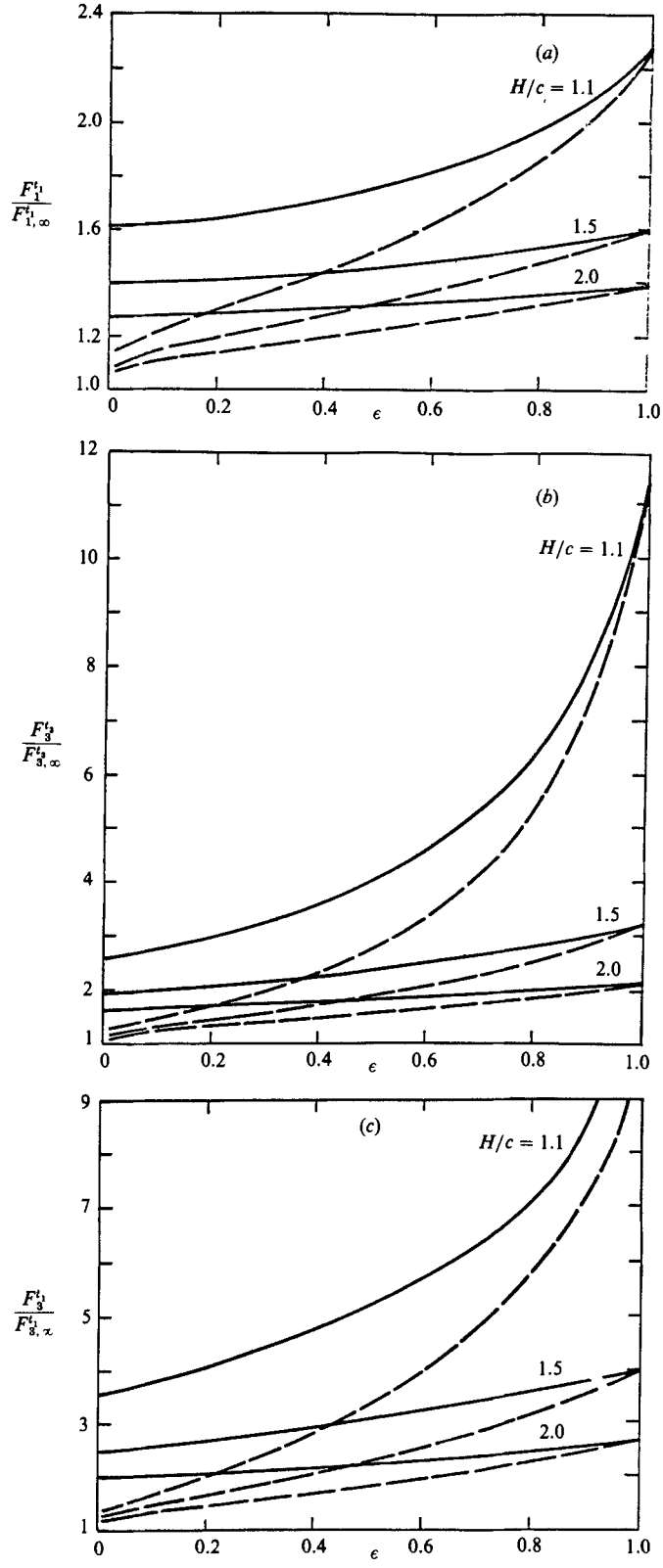

FIGURE 13. Resistance coefficients (*a*) $F_1^{t_1}$, (*b*) $F_3^{t_3}$ and (*c*) $F_3^{t_1}$ for a spheroid inclined at an orientation $\alpha = 45°$ in the vicinity of a planar wall as a function of aspect ratio ϵ. ——, oblate; – – –, prolate.

		Boundary integral method (present work)			Method of reflections Wakiya (1959)		
	H/b	$\alpha = 0°$	$\alpha = 45°$	$\alpha = 90°$	$\alpha = 0°$	$\alpha = 45°$	$\alpha = 90°$
(*a*)	1.1	2.08	1.75	1.574	1.77	1.57	1.345
	1.5	1.530	1.455	1.380	1.488	1.415	1.346
	2.0	1.343	1.309	1.269	1.333	1.298	1.259
	2.5	1.256	1.234	1.208	1.252	1.230	1.204
	5.0	1.113	1.106	1.097	1.113	1.106	1.097
	10.0	1.054	1.051	1.047	1.054	1.051	1.047
(*b*)	1.1	7.18	5.23	4.59	1.54	1.31	1.13
	1.5	3.21	3.096	2.86	2.282	2.222	2.172
	2.0	2.269	2.265	2.265	2.023	2.031	2.043
	2.5	1.886	1.899	1.911	1.790	1.807	1.826
	5.0	1.349	1.358	1.367	1.342	1.351	1.361
	10.0	1.156	1.160	1.164	1.156	1.160	1.164
(*c*)	1.1	−0.228	−0.0514	−0.0591	−0.126	−0.00870	−0.0897
	1.5	−0.0656	−0.0155	0.0325	−0.0572	−0.00796	−0.0453
	2.0	−0.0302	−0.00603	0.0189	−0.0288	−0.00409	0.0238
	2.5	−0.0177	−0.00307	0.0124	−0.0173	−0.00233	0.0146
	5.0	−0.00385	−0.00048	0.0032	−0.00385	−0.00044	0.0033
	10.0	−0.00091	−0.000096	0.00078	−0.00091	−0.000094	0.00079

TABLE 3. Comparison of values of (*a*) $F_1^{t_1}/F_{1,\infty}^{t_1}$, (*b*) $F_3^{t_3}/F_{3,\infty}^{t_3}$, and (*c*) $T_2^{t_1}$ obtained by the present boundary integral method to values obtained by the method of reflections for an oblate spheroid with $a/b = 0.5$

as shown in figure 10. For an oblate spheroid the ratio is less than unity for small α and is greater than unity for large α. When α approaches 90° the ratio of $T_2^{t_3}/T_{2,\infty}^{t_3}$ increases very rapidly. When the aspect ratio is very small ($\epsilon = 0.1$) and α is very close to 90°, $T_2^{t_3}/T_{2,\infty}^{t_3}$ becomes very large although the actual value of $T_2^{t_3}$ at $\alpha = 90°$ is much less than the value at $\alpha = 0°$. For a prolate spheroid the ratio $T_2^{t_3}/T_{2,\infty}^{t_3}$ has its maximum value at $\alpha = 0°$ for a given spacing.

The dimensionless torque coefficients for parallel and perpendicular motion are shown in figures 11 and 12, respectively. As expected both coefficients vanish when $H/c \to \infty$. It is interesting to note that the torque due to the parallel motion changes sign as a function of the orientation angle. Therefore for each particle-to-wall spacing and aspect ratio, there is a critical orientation angle for which a spheroid can translate parallel to the wall without experiencing any torque.

Comparing the corresponding curves for a prolate and oblate spheroid having the same aspect ratio we find that the qualitative variation of all the coefficients with α for a prolate spheroid is similar to that for an oblate spheroid having the same aspect ratio at an orientation of $90° - \alpha$. This is because while the angle between the major axis and the wall is α for a prolate spheroid, it is $90° - \alpha$ for an oblate spheroid.

In order to more clearly see the effect of body shape, figure 13 shows the force coefficients $F_1^{t_1}$, $F_3^{t_3}$ and $F_3^{t_1}$ as a function of the aspect ratio ϵ at $\alpha = 45°$ and several constant values of H/c. All three ratios have their maximum values for a sphere ($\epsilon = 1$). The coefficient $F_3^{t_1}$ is zero for a sphere. When ϵ approaches unity the ratio $F_3^{t_1}/F_{3,\infty}^{t_1}$ increases with ϵ very rapidly but has limiting values. For a spheroid with ϵ close to unity the absolute value of $F_3^{t_1}$ is very small and converges much slower

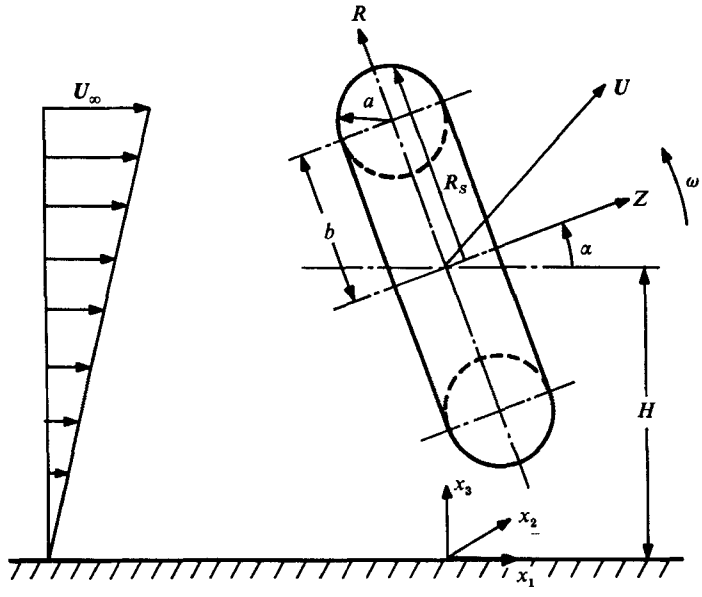

FIGURE 14. Geometry for the motion of a torus near a planar wall.

than other coefficients. Limited by computer time, the values of $F_3^{t_1}$ have not been calculated accurately for ϵ very close to unity at $H/c = 1.1$ and, therefore, are not shown in figure 13(*c*).

The force and torque coefficients of a spheroid moving parallel to a wall have been obtained by the method of reflections in Wakiya (1959). The results achieved by the method of reflections are compared to the solutions of the present boundary-integral method in table 3. At large spacings the results of Wakiya are in good agreement with the values achieved by the boundary-integral method. At close spacings the discrepancy increases, but agreement is still good for the coefficient $F_1^{t_1}$ up to $H/b = 1.5$. For the coefficients $F_3^{t_1}$ and $T_2^{t_1}$ the results obtained by the method of reflections have substantial error at close spacings. For example, at $H/b = 1.5$ and 1.1 the value of $F_3^{t_1}$ calculated by the method of reflections is 25% and four times less respectively than the strong-interaction solutions obtained by the present theory. Even at $H/b = 5$ the error of the values of $T_2^{t_1}$ computed by the method of reflections is close to 10%.

4. Solutions for the motion of a torus near a planar wall

The creeping motion of a torus in a viscous fluid near an infinite planar wall is illustrated in figure 14. The particle has a translational velocity $\boldsymbol{U}_0$ and is rotating with an angular velocity ω. $\boldsymbol{U}_\infty$ represents the undisturbed simple shear flow.

In §2, a theory was developed for treating any arbitrary body of revolution whose surface could be expressed by the single-valued function $R_S(Z)$, where the Z-axis lies along the particle axis of symmetry. However, the torus currently under consideration and the biconcave-shaped disc to be treated in the next section are examples of a body of revolution whose shape R_S is a multivalued function of Z. Therefore, a modification of the theory presented in §2 is needed. Accordingly, we

choose a suitable parameter η so that both R_S and Z are related to it by a single-valued function. For the case of a torus:

$$\left.\begin{aligned} R_S &= b + a\sin\eta, \\ Z &= a\cos\eta, \end{aligned}\right\} \quad 0 \leqslant \eta < 2\pi \tag{4.1a}$$

(4.1b)

The outside portion of the torus is represented by varying η from 0° to 180° while the inside portion by varying η from 180° to 360°. The stokeslet density functions for motion having planar symmetry are represented by the double Fourier series:

$$\left.\begin{aligned} f_1 &= \sum_{m=0}^{\infty}\left\{A_{1,m,0} + \sum_{n=1}^{\infty}(A_{1,m,n}\cos n\eta + B_{1,m,n}\sin n\eta)\right\}\cos m\theta, \\ f_2 &= \sum_{m=1}^{\infty}\left\{A_{2,m,0} + \sum_{n=1}^{\infty}(A_{2,m,n}\cos n\eta + B_{2,m,n}\sin n\eta)\right\}\sin m\theta, \\ f_3 &= \sum_{m=0}^{\infty}\left\{A_{3,m,0} + \sum_{n=1}^{\infty}(A_{3,m,n}\cos n\eta + B_{3,m,n}\sin n\eta)\right\}\cos m\theta. \end{aligned}\right\} \tag{4.2}$$

Substituting (4.1 a, b) and (4.2) into the integral equation (2.15), all integrals can be performed with respect to the variables θ and η. The integration along the θ-direction is performed analytically as shown in Appendix A. The integration in the η-direction is performed numerically. After the coefficients $A_{k,m,n}$ and $B_{k,m,n}$ are obtained, the drag and torque on the particle are found to be

$$F_k = 2\pi^2 a\,(2bA_{k,0,0} + aB_{k,0,1}), \quad k = 1 \quad \text{and} \quad 3. \tag{4.3}$$

$$\begin{aligned} T_2 = \pi^2\{&-(a^2+2b^2)\,(A_{1,1,0}\cos\alpha + A_{3,1,0}\sin\alpha) \\ &+ 2ab\,[(A_{3,0,1} - B_{1,1,1})\cos\alpha - (A_{1,0,1} + B_{3,1,1})\sin\alpha] \\ &+ a^2\,[(\tfrac{1}{2}A_{1,1,2} + B_{3,0,2})\cos\alpha + (\tfrac{1}{2}A_{3,1,2} + B_{3,0,2})\sin\alpha]\}. \end{aligned} \tag{4.4}$$

The hydrodynamic force and torque coefficients for a torus in the vicinity of a planar wall are defined as follows:

$$\begin{pmatrix} F_1 \\ F_3 \\ T_2 \end{pmatrix} = 6\pi\mu c \begin{pmatrix} F_1^{t_1} & F_1^{t_3} & F_1^{r} & HF_1^{S} \\ F_3^{t_1} & F_3^{t_3} & F_3^{r} & HF_3^{S} \\ \frac{4}{3}cT_2^{t_1} & \frac{4}{3}cT_2^{t_3} & \frac{4}{3}cT_2^{r} & \frac{2}{3}c^2T_2^{S} \end{pmatrix} \begin{pmatrix} U_1 \\ U_3 \\ c\omega \\ S \end{pmatrix}, \tag{4.5}$$

where $c = a + b$ is the outer radius of the torus.

The force and torque coefficients for the translational and rotational motion of a torus in an otherwise unbounded quiescent fluid are listed in Goren & O'Neill (1980). For reference the force and torque coefficients for a torus with $b/a = 2$ and 10 are listed in table 4. These values are also calculated using the present boundary-integral method and are found to be in full agreement with the exact solution. To the best of the authors' knowledge the torque coefficient for a torus in an unbounded shear flow has not previously been computed. The values of this coefficient presented in table 4 have been calculated using the present theory.

When the axis of symmetry is perpendicular to the wall the coefficient matrix (2.15) is independent of θ and only one-dimensional collocation is needed as illustrated in Apprendix B for a sphere. The collocation points, each of which represents a ring on the particle surface on which the no-slip boundary conditions are exactly satisfied, are chosen by specifying equally spaced values of η in the range 0° and 360°. Tables

	$b/a = 2$	$b/a = 10$
Force coefficient for motion parallel to symmetry axis	−0.9072	−0.7843
Force coefficient for motion perpendicular to symmetry axis	−0.7732	−0.6174
Torque coefficient for a torus rigidly held in a shear flow parallel to the symmetry axis	−0.9477	−0.8440
Torque coefficient for a torus rigidly held in a shear flow perpendicular to the symmetry axis	−0.1703	−0.01678
Torque coefficient for rotation about an axis perpendicular to the symmetry axis	−0.5590	−0.4304

TABLE 4. Force and torque coefficients for a torus in an infinite fluid

(*a*) $b/a = 2$

$N\backslash H/c$	0.5	0.8	1.1	1.5	∞
4	−25.15	−5.921	−3.677	−2.150	−0.9174
6	−19.60	−5.500	−3.111	−2.136	−0.9072
8	−18.30	−5.499	−3.121	−2.140	−0.9072
10	−18.42	−5.500	−3.122	−2.141	−0.9072
12	−18.52	−5.500	−3.122	−2.141	—
14	−18.51	−5.500	—	—	—
16	−18.51	—	—	—	—

(*b*) $b/a = 10$

$N\backslash H/c$	0.2	0.5	0.8	1.1	1.5	∞
4	−9.122	−3.120	−2.167	−1.741	−1.348	−0.7823
6	−7.547	−2.858	−2.142	−1.764	−1.471	−0.7843
8	−7.232	−2.859	−2.140	−1.764	−1.471	−0.7843
10	−7.233	−2.859	−2.140	—	—	—
12	−7.233	—	—	—	—	—

TABLE 5. Convergence of the coefficient $F_3^{t_3}$ for a torus with its symmetry axis perpendicular to the wall

(*a*) $b/a = 2$

$N\backslash H/c$	0.5	0.8	1.1	1.5	∞
4	−3.124	−1.542	−1.312	−1.118	−0.7706
6	−1.881	−1.366	−1.170	−1.048	−0.7732
8	−2.063	−1.372	−1.171	−1.048	−0.7732
10	−2.077	−1.372	−1.171	−1.048	−0.7732
12	−2.079	−1.372	−1.171	—	—
14	−2.079	—	—	—	—
16	−2.079	—	—	—	—

(*b*) $b/a = 10$

$N\backslash H/c$	0.2	0.5	0.8	1.1	1.5	∞
4	−2.534	−1.006	−0.9103	−0.8311	−0.7737	−0.6166
6	−1.910	−1.096	−0.9132	−0.8324	−0.7749	−0.6174
8	−1.927	−1.096	−0.9132	−0.8324	−0.7749	−0.6174
10	−1.928	−1.096	—	—	—	—
12	−1.928	—	—	—	—	—

TABLE 6. Convergence of the coefficient $F_1^{t_1}$ for a torus with its symmetry axis perpendicular to the wall

(a) $b/a = 2$

$N\backslash H/c$	0.5	0.8	1.1	1.5	∞
4	−2.943	−0.9314	−0.7724	−0.6734	−0.5810
6	−1.774	−0.8890	−0.6997	−0.6228	−0.5584
8	−2.262	−0.9175	−0.7071	−0.6230	−0.5590
10	−2.319	−0.9176	−0.7071	−0.6230	−0.5590
12	−2.323	−0.9176	−0.7071	−0.6230	—
14	−2.324	−0.9176	—	—	—
16	−2.324	—	—	—	—

(b) $b/a = 10$

$N\backslash H/c$	0.2	0.5	0.8	1.1	1.5	∞
4	−2.847	−0.8657	−0.6231	−0.5320	−0.4915	−0.4408
6	−2.226	−0.8223	−0.6044	−0.5219	−0.4748	−0.4304
8	−2.227	−0.8224	−0.6044	−0.5219	−0.4748	−0.4304
10	−2.229	−0.8224	−0.6044	—	—	—
12	−2.229	—	—	—	—	—

TABLE 7. Convergence of the coefficient T_2^r for a torus with its symmetry axis perpendicular to the wall

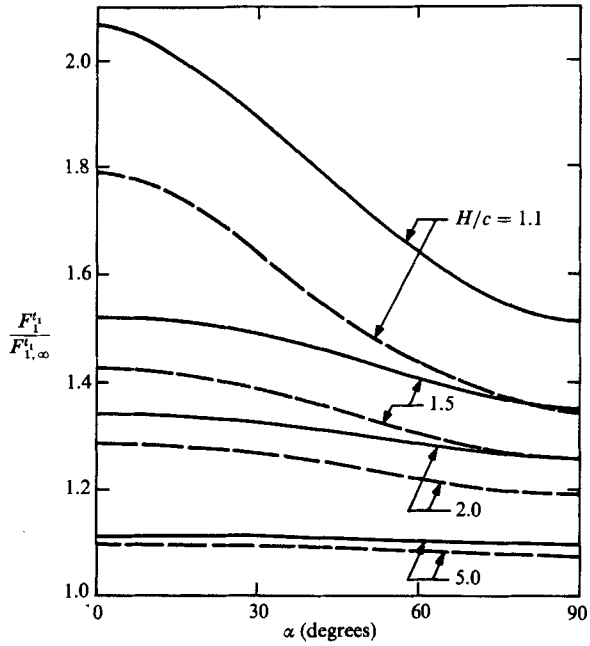

FIGURE 15. The drag force on a torus moving parallel to a wall. ——, $b/a = 2$, – – –. $b/a = 10$.

5–7 show convergence tests for the coefficients $F_3^{t_3}$, $F_1^{t_1}$ and T_2^r for a torus having $b/a = 2$ and 10. The values of the coefficients in an infinite fluid rapidly converge to the exact solutions using only eight collocation points. As expected more collocation points are needed to get the same accuracy when the particle is close to the wall. Convergence is somewhat slower for $b/a = 2$ than for $b/a = 10$. In the worst case tested ($b/a = 2$, $H/c = 0.5$) only 14 collocation points are required to achieve four-digit accuracy for all the force and torque coefficients.

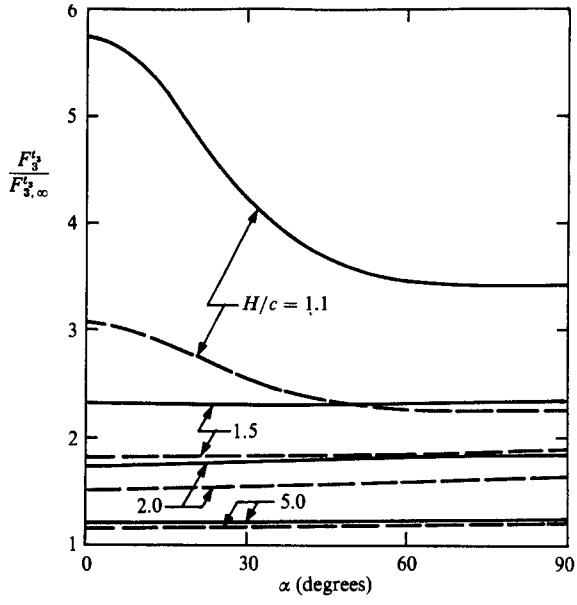

FIGURE 16. The drag force on a torus moving perpendicular to a wall. ——, $b/a = 2$, – – –, $b/a = 10$.

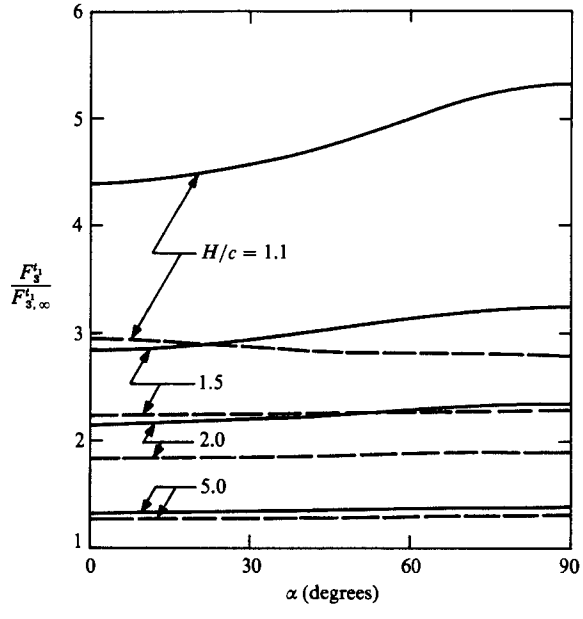

FIGURE 17. The force component perpendicular to the wall on a torus translating parallel to the wall. ——, $b/a = 2$, – – –, $b/a = 10$.

Theoretical values of the ratio $F_1^{t_1}/F_{1,\infty}^{t_1}$ have been obtained by Kucaba-Pietal (1986) for a torus translating parallel to the wall with its axis of symmetry oriented perpendicular to the wall for $H/c \geqslant 1.13$ using the multipole technique. Figure 4 of Kucaba-Pietal (1986) which presents these results was plotted incorrectly (A. Kucaba-Pietal 1987, private communication). In order for the results in this figure

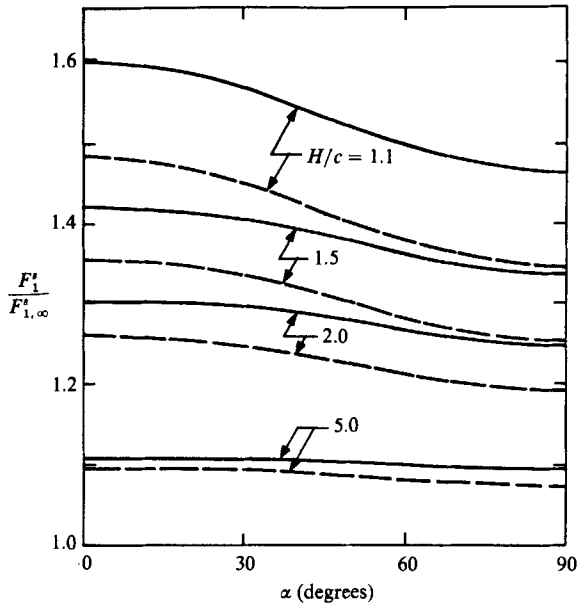

FIGURE 18. The force component parallel to the wall on a torus which is rigidly held in a shear flow in the vicinity of a planar wall. ——, $b/a = 2$, – – –, $b/a = 10$.

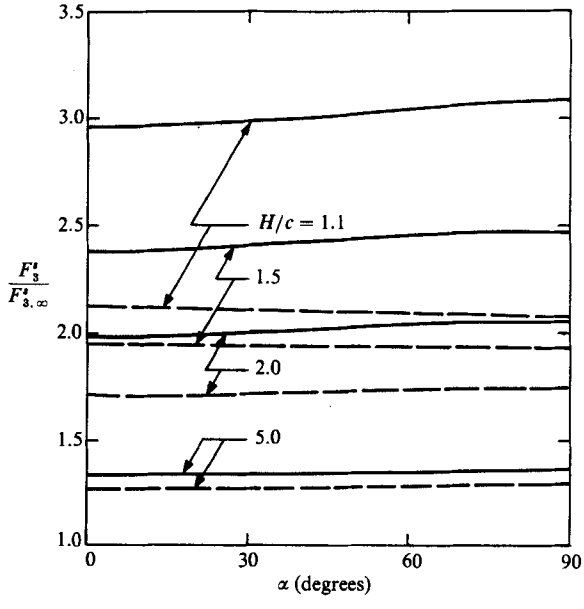

FIGURE 19. The force component perpendicular to the wall on a torus which is rigidly held in a shear flow in the vicinity of a planar wall. ——, $b/a = 2$, – – –, $b/a = 10$.

to make sense, the parameter T defined as the outer diameter of the torus is actually the outer radius of the torus. With this correction, the converged solutions shown in table 6 are in good agreement with the multipole calculations of Kucaba-Pietal (1986) for the spacings $H/c \geqslant 1.13$ where solutions are available.

When the torus is arbitrarily oriented relative to the wall, the general two-

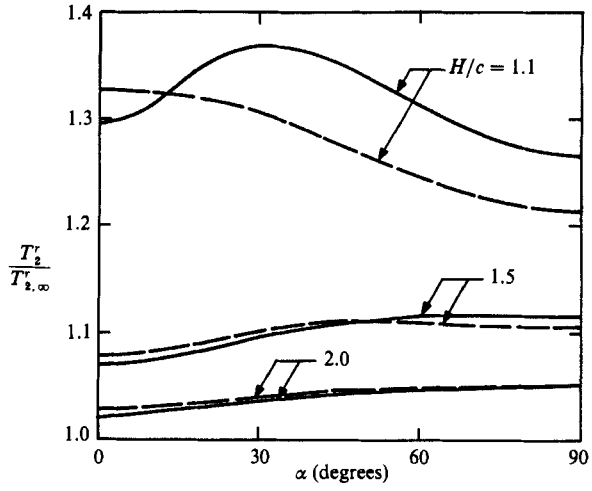

FIGURE 20. Torque on a rotating torus near a planar wall. ——, $b/a = 2$, – – –, $b/a = 10$.

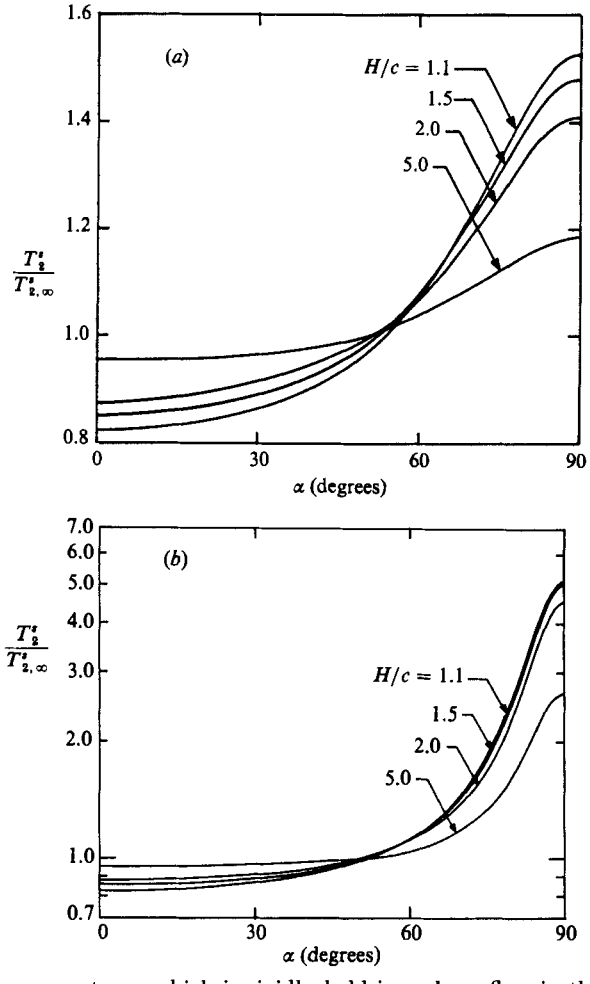

FIGURE 21. Torque on a torus which is rigidly held in a shear flow in the vicinity of a planar wall. (*a*) $b/a = 2$, (*b*) $b/a = 10$.

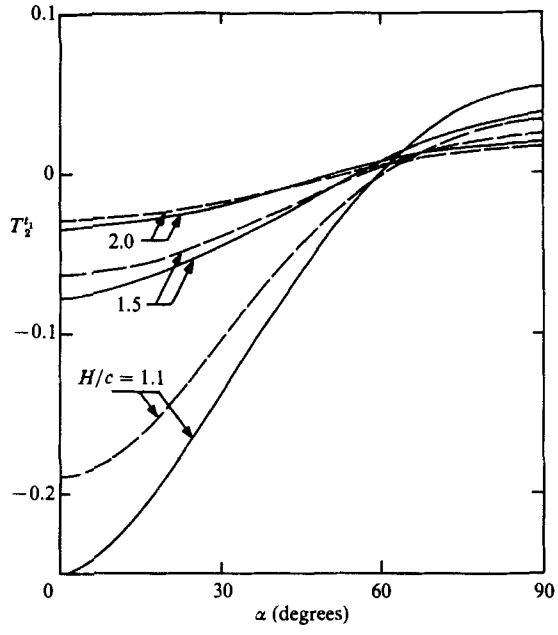

FIGURE 22. Torque on a torus translating parallel to a wall. —, $b/a = 2$, – – –, $b/a = 10$.

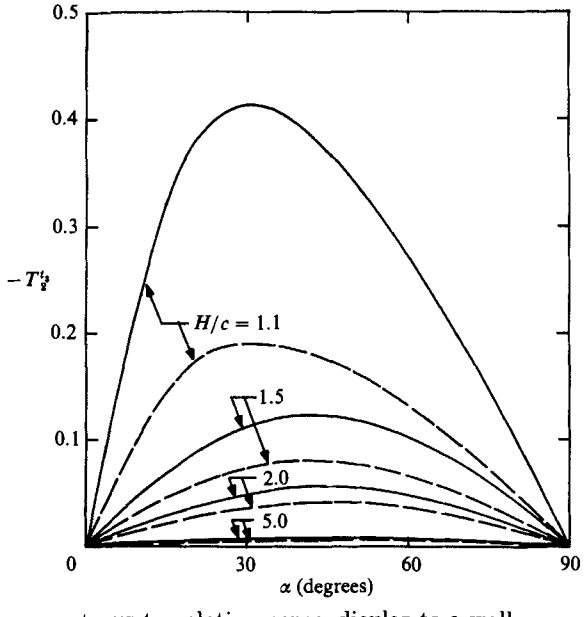

FIGURE 23. Torque on a torus translating perpendicular to a wall. ——, $b/a = 2$, – – –, $b/a = 10$.

dimensional collocation is needed. The collocation points are placed at equally spaced values of η between 0° and 360°. A constant value of η represents a ring on the particle surface. At each ring the points are equally spaced between $\theta = 0°$ and 180°. Convergence tests of the force and torque coefficients for a torus having $a/b =$ 0.1 and 0.5 (see figure 14) with respect to the wall were performed and the rate of convergence was found to be similar to that of an oblate spheroid whose results are

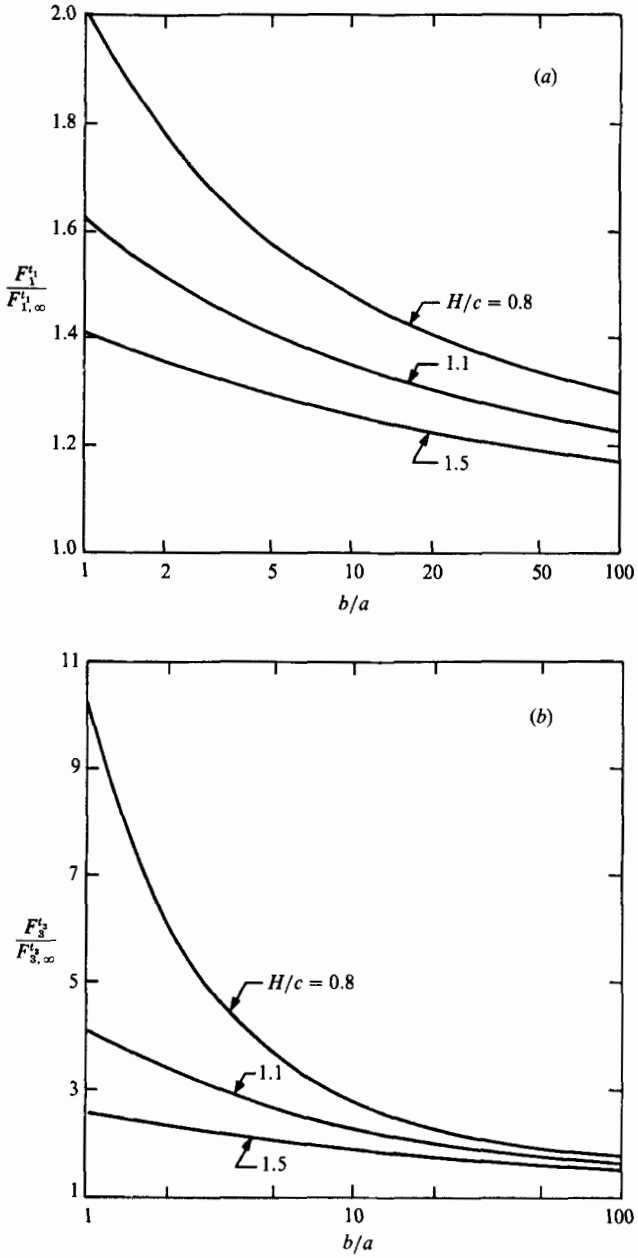

FIGURE 24. Resistance coefficients (*a*) $F_1^{t_1}$ and (*b*) $F_3^{t_2}$ for a torus with its symmetry axis oriented perpendicular to a wall as a function of b/a.

shown in table 2. The actual numerical values of these convergence tests for an inclined torus are contained in Hsu (1985).

Figures 15–23 show converged values of the nine independent coefficients for a torus with $b/a = 2$ and 10 as a function of orientation angle α and the separation distance H/c.

Comparing the curves for a torus of $b/a = 2$ with those for an oblate spheroid having aspect ratio $\epsilon = 0.5$ presented in §3, most of the curves having the same value

of H/c exhibit similar behaviour qualitatively and quantitatively especially for small values of the orientation angle α. The only exception is the ratio $F_3^{t_1}/F_{3,\infty}^{t_1}$, which increases with increasing α for a torus while it decreases with increasing α for an oblate spheroid. Although the ratio of $F_3^{t_1}/F_{3,\infty}^{t_1}$ is substantially different for the torus and the oblate spheroid at $H/c = 1.1$, the ratio becomes relatively insensitive to orientation angle for $H/c > 2$, and for a given value of H/c the two ratios are approximately equal. In an unbounded fluid the difference between the corresponding values of the actual resistance coefficients for both shapes is less than 1 %. Therefore an oblate spheroid having aspect ratio $\epsilon = 0.5$ can be used as a good approximation of the motion of a torus with $b/a = 2$ when the torus is not very close to the wall. It is worth noting that an oblate spheroid with $\epsilon = 0.5$ and a torus with $b/a = 2$ having the same outer radius have approximately same surface area. On the other hand the motion of a torus having $b/a = 10$ would not be similar to the motion of an oblate spheroid even in an unbounded fluid.

Finally figure 24 shows the variation of $F_1^{t_1}/F_{1,\infty}^{t_1}$ and $F_3^{t_3}/F_{3,\infty}^{t_3}$ as functions of b/a for a torus with its axis of symmetry oriented perpendicular to the wall. Both ratios decrease with increasing aspect ratio. As expected, the ratio $F_3^{t_3}/F_{3,\infty}^{t_3}$ is a much stronger function of the aspect ratio than is the ratio $F_1^{t_1}/F_{1,\infty}^{t_1}$.

5. Solutions for the motion of a biconcave-shaped body near a planar wall

The typical shape of an undeformed red blood cell is shown in figure 25. The shape can be expressed as

$$B = R_0(1-R_S^2)^{\frac{1}{2}}(C_0+C_1R_S^2+C_2R_S^4), \tag{5.1}$$

where B is the width, R_S is the radius of the blood cell, R_0, C_0, C_1 and C_2 are constants, and R_0 represents the largest radius. Representative values of these constants are listed in Fung (1981). In this section we solve for the motion of a blood cell adjacent to a planar wall using the values

$$R_0 = 3.91\mu, \quad C_0 = 0.81\mu, \quad C_1 = 7.83\mu, \quad C_2 = 4.39\mu. \tag{5.2}$$

As in the case of a torus the shape $R = R(Z)$ is not a single-valued function. To describe the biconcave shape we introduce a new parameter η and let

$$R_S = R_0\cos\eta, \tag{5.3a}$$

$$Z = \tfrac{1}{2}R_0(1-R_S^2)^{\frac{1}{2}}(C_0+C_1R_S^2+C_2R_S^2)\operatorname{sgn}\eta, \tag{5.3b}$$

where $\operatorname{sgn}(x) = |x|/x$. Then both R_S and Z are single-valued functions of η. The stokeslet density functions are represented by the double Fourier–Legendre series:

$$\left.\begin{aligned} f_1 &= \sum_{m=0}^{\infty}\sum_{n=0}^{\infty} A_{1,m,n}P_n(\cos\eta)\cos m\theta, \\ f_2 &= \sum_{m=1}^{\infty}\sum_{n=0}^{\infty} A_{2,m,n}P_n(\cos\eta)\sin m\theta, \\ f_3 &= \sum_{m=0}^{\infty}\sum_{n=0}^{\infty} A_{3,m,n}P_n(\cos\eta)\cos m\theta, \end{aligned}\right\} \tag{5.4}$$

where $P_n(x)$ is the Legendre function of order n. Substituting (5.3a, b) and (5.4) into integral equation (2.15) all integrals in (2.15) can be performed with respect to the variables θ and η, as was done for the torus. The collocation points are arranged such

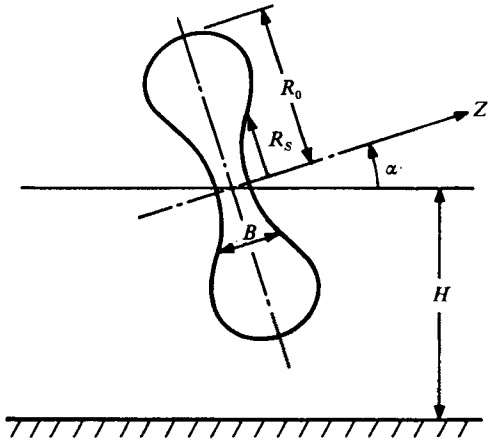

FIGURE 25. Geometry of a biconcave shaped disc near a planar wall.

Force coefficient for motion parallel to symmetry axis	−0.9062
Force coefficient for motion perpendicular to symmetry axis	−0.7724
Torque coefficient for the body rigidly held in a shear flow parallel to the symmetry axis	−0.9460
Torque coefficient for the body rigidly held in a shear flow perpendicular to the symmetry axis	−0.1676
Torque coefficient for rotation about an axis perpendicular to the symmetry axis	−0.5568

TABLE 8. Force and torque coefficients for the biconcave-shaped disc in an infinite fluid.

that the rings, which are represented by constant values of η, are nearly equally spaced along the arclength of the body shown in figure 25 and somewhat more concentrated in the vicinity of maximum radius. At each ring the collocation points are equally spaced between $\theta = 0°$ and 180°. The convergence behaviour of the force and torque coefficients is similar to the case of a torus having $b/a = 2$.

The hydrodynamic force and torque coefficients of the biconcave-shaped disc are defined as follows:

$$\begin{pmatrix} F_1 \\ F_3 \\ T_2 \end{pmatrix} = 6\pi\mu R_0 \begin{pmatrix} F_1^{t_1} & F_1^{t_3} & F_1^{r} & HF_1^{S} \\ F_3^{t_1} & F_3^{t_3} & F_3^{r} & HF_3^{S} \\ \frac{4}{3}R_0 T_2^{t_1} & \frac{4}{3}R_0 T_2^{t_3} & \frac{4}{3}R_0 T_2^{r} & \frac{2}{3}R_0^2 T_2^{S} \end{pmatrix} \begin{pmatrix} U_1 \\ U_3 \\ R_0\omega \\ S \end{pmatrix}. \tag{5.5}$$

The values of the force and torque coefficients for the biconcave-shaped disc described by (5.1) and (5.2) in an infinite fluid, obtained using the present theory, are listed in table 8. All the coefficients are remarkably close to the corresponding values for a torus with $b/a = 2$. When a planar wall is present the numerical solutions show that the force and torque coefficients are still quite close for the two bodies having the same H/c and α. The difference between them is less than 1% for all nine force

and torque coefficients for separation distances as close as $H/c = 1.1$. Therefore figures 15–23 can also be used to predict the force and torque of a biconcave-shaped body described by (5.1) and (5.2) to a high degree of accuracy. It is worth noting that the biconcave-shaped body and a torus with $b/a = 2$ have the same surface area if their outer radii are the same. The coincidence of the force and torque shows that the hole in a torus of $b/a = 2$ has little influence on the flow field. As mentioned in §4 an oblate spheroid having aspect ratio $\epsilon = 0.5$ can also serve as a good approximation for the motion of a torus of $b/a = 2$ when it is not very close to the wall.

6. Concluding remarks

The successful application of the boundary-integral method to the motion of a spheroid, a torus and a biconcave-shaped disc near a planar wall has shown that the method is effective and suitable for treating the motion of a body of arbitrary shape near boundaries. Examples of the types of problems that can be treated include the motion of a non-spherical particle between two walls or in a circular cylinder. The method is also suitable for treating deformable bodies such as a fluid droplet (Rallison & Acrivos 1978), or a deformable interface between two immiscible fluids (Leal & Lee 1982*a*, *b*).

A limitation of the technique is the long computation time required to evaluate the double integrals in the integral equations. Therefore great effort has been taken in this study to evaluate all the integrals in the azimuthal direction analytically. In this way a tremendous amount of computational time has been saved and the accuracy of the solution is greatly increased.

In closing, the authors wish to mention that the solutions for the force and torque coefficients obtained in the present study have been applied to obtain the trajectories of an oblate spheroidal particle settling under gravity adjacent to an inclined planar surface and of a neutrally buoyant spheroid in shear flow adjacent to a planar wall. The motion of a non-spherical particle is much more complicated than the motion of a sphere because of the dependence of the resistance force on the orientation and the fact that some coupling forces are not identically zero as in the case of a spherical particle. This work is to be submitted for publication shortly.

This research was supported by a Research Initiation Grant from the National Science Foundation, No. CME81-05914 and by a grant from The City University of New York PSC-CUNY Research Award Program, No. 6-63244(FY-14). Their support is gratefully acknowledged. The authors also wish to thank the City University of New York Computer Center and The City College of New York Computer Center for the use of their facilities. The above work has been performed in partial fulfillment of the requirements for the Ph.D. degree of R. Hsu from The Graduate School of The City University of New York.

Appendix A

A key step in keeping computation time at a minimum while maintaining high accuracy is to evaluate the integrals in (2.15) analytically in the θ-direction. After lengthy algebraic operations all of the required integrals in the θ-direction can be reduced to the following general form:

$$I = \int_0^{2\pi} \frac{\cos m\theta \, \mathrm{d}\theta}{[A - B\cos\theta]^{p/2}}, \tag{A 1}$$

where m is 0 or an integer and $p = 1, 3, 5$ and 7. This integral can also be written as

$$I = \frac{4}{(A+B)^{p/2}} Q(K, m, p, \tfrac{1}{2}\pi) \tag{A 2}$$

where

$$Q(K, m, p, \theta) = \int_0^\theta \frac{\cos 2mt \, dt}{[1-K^2 \sin^2 t]^{p/2}}, \tag{A 3}$$

$$K^2 = \frac{2B}{A+B} \leqslant 1. \tag{A 4}$$

To evaluate the integral $Q(K, m, p, \theta)$ we discuss two cases.

(*a*) $0.8 < K < 1$: This integral can be represented by the series

$$Q(K, m, p, \theta) = \sum_{i=0}^{m} \alpha_{mi} G(K, p, i, \theta), \tag{A 5}$$

where

$$\alpha_{mi} = \begin{cases} 1 & i = m = 0 \\ m \dfrac{(-1)^i 2^{2i} (m+i-1)!}{(2i)!\,(m-i)!} & \text{otherwise,} \end{cases} \tag{A 6}$$

$$G(K, p, i, \theta) = \int_0^\theta \frac{\cos^{2i} t \, dt}{(1-K^2 \sin^2 t)^{p/2}}. \tag{A 7}$$

The function $G(K, p, i, \theta)$ can be expressed in terms of elliptic functions of the first and second kind as follows:

$$G(K, -1, 0, \theta) = E(\theta, K), \tag{A 8}$$

$$G(K, 1, 0, \theta) = F(\theta, K), \tag{A 9}$$

$$G(K, p, 0, \theta) = -\frac{K^2 \sin\theta \cos\theta}{(p-2) K'^2 \Delta^{p-2}} + \frac{(p-3)(2-K^2)}{(p-2) K'^2} G(K, p-2, 0, \theta) - \frac{p-4}{(p-2) K'^2} G(K, p-4, 0, \theta), \tag{A 10}$$

$$G(K, p, i, \theta) = \frac{1}{K^2} G(K, p-2, i-1, \theta) - \frac{K'^2}{K^2} G(K, p, i-1, \theta), \tag{A 11}$$

where E and F are incomplete elliptic functions of the first and second kind, respectively, $K'^2 = 1-K^2$ and $\Delta = (1-K^2 \sin^2\theta)^{\frac{1}{2}}$.

Unfortunately the results given by (A 5) produce large round-off error for small K and large m. Therefore (A 5) can be used only for K close to unity.

(*b*) $0 < K < 0.8$: When K is not close to unity we use the infinite series

$$(1-K^2 \sin^2\theta)^{-n/2} = 1 + \tfrac{1}{2} n K^2 \sin^2\theta + \tfrac{1}{2}[\tfrac{1}{2} n (\tfrac{1}{2} n + 1)] K^4 \sin^4\theta + \ldots + \frac{(\frac{1}{2} n)(\frac{1}{2} n + 1) \ldots (\frac{1}{2} n + J - 1)}{J!} K^{2J} \sin^{2J}\theta + \ldots. \tag{A 12}$$

Then using the known result

$$\int_0^{\pi/2} \sin^{2J} x \cos 2mx \, dx = \begin{cases} \dfrac{\pi(-1)^m}{2^{2m-1}} \dbinom{2J}{J-m}, & J \geqslant m \\ 0, & J < m, \end{cases} \tag{A 13}$$

we get

$$Q(K,m,p,\tfrac{1}{2}\pi) = \frac{(-1)^m\pi}{2^{2m-1}} \sum_{J=m}^{\infty} \binom{2J}{J-m} \frac{\frac{1}{2}p\,(\frac{1}{2}p+1)\ldots(\frac{1}{2}p+J-1)\,K^{2J}}{J!}. \tag{A 14}$$

The infinite series (A 14) converges very quickly for K not close to unity.

The applicable regions for K of equations (A 5) and (A 14) overlap. Numerical tests show that $K = 0.8$ is a reasonable value for matching the two solutions.

When $Z = Z^*$ and $\theta = \theta^*$ the following integrals in (2.15) become singular:

$$\iint_{S_p} \left(\frac{1}{r} - \frac{r_i r_k}{r^3}\right) f_k(\boldsymbol{x})\,\mathrm{d}S_x \tag{A 15}$$

and

$$\iint_{S_p} \frac{r_i r_j r_k}{r^5} v_k(\boldsymbol{x})\, n_j(\boldsymbol{x})\,\mathrm{d}S_x. \tag{A 16}$$

To evaluate these integrals we divide the region of integration into four subregions as follows:

$$\int_{-a}^{+a}\int_0^{2\pi} \phi\,\mathrm{d}\theta\,\mathrm{d}Z = \left(\int_{-a}^{Z^*-\epsilon}\int_0^{2\pi} + \int_{Z^*+\epsilon}^{a}\int_0^{2\pi} + \int_{Z^*-\epsilon}^{Z^*+\epsilon}\int_{\epsilon_1}^{2\pi-\epsilon_1} + \int_{Z^*-\epsilon}^{Z^*+\epsilon}\int_{-\epsilon_1}^{\epsilon_1}\right)\phi\,\mathrm{d}\theta\,\mathrm{d}Z \tag{A 17}$$

where $0 < \epsilon \ll a$, $\epsilon_1 = \epsilon/R_0$. The first three integrals on the right-hand side of (A 17) are regular, while the fourth is singular. The first two integrals in the θ-direction can be evaluated using (A 5) or (A 14). The third one can be represented by

$$\int_0^{2\pi-\epsilon_1} \frac{\cos 2m\theta\,\mathrm{d}\theta}{(1-K^2\sin^2\theta)^{p/2}} = 4\sum_{i=0}^{m} \alpha_{mi}\, G(K,p,i,\tfrac{1}{2}(\pi-\epsilon_1)) \tag{A 18}$$

where the function $G(K,p,i,\frac{1}{2}(\pi-\epsilon_1))$ can be expressed in terms of the incomplete elliptic functions by (A 8)–(A 11). The last one can be evaluated analytically by treating the small region around the singularity as a flat plane as was done by Youngren & Acrivos (1975).

Appendix B

To test the accuracy and convergence characteristics of the solution technique, we consider the following elementary problems involving the motion of a spherical body adjacent to a planar wall where exact solutions are available for comparison: (1) pure translation of a sphere perpendicular to the wall; (2) pure translation of a sphere parallel to the wall; (3) pure rotation of a sphere about an axis parallel to the wall; (4) shear flow past a rigidly held sphere near the wall.

We first look at pure axisymmetric translation of the sphere perpendicular to the wall. With $\alpha = 90°$, (see figure 3) the stress forces in the R- and Z-directions must be independent of the aximuthal angle θ and the stress forces in the azimuthal direction are identically zero. So, we set:

$$\left.\begin{aligned} f_1 &= \sum_{n=0}^{\infty} A_n P_n\left(\frac{Z}{a}\right)\cos\theta, \\ f_2 &= \sum_{n=0}^{\infty} A_n P_n\left(\frac{Z}{a}\right)\sin\theta, \\ f_3 &= \sum_{n=0}^{\infty} C_n P_n\left(\frac{Z}{a}\right). \end{aligned}\right\} \tag{B 1}$$

	(*a*)				(*b*)			
$N\backslash H/a$	1.1276	1.5431	2.3524	3.7622	1.1276	1.5431	2.3524	3.7622
5	−32.13	−3.039	−1.839	−1.222	−8.38	−3.035	−1.837	−1.222
7	−12.09	−3.036	−1.838	−1.222	−9.05	−3.036	−1.838	−1.222
9	−9.45	−3.036	−1.838	—	−9.21	−3.036	−1.838	—
11	−9.25	—	—	—	−9.24	—	—	—
13	−9.25	—	—	—	−9.25	—	—	—
Exact	−9.25	−3.036	−1.838	−1.222	−9.25	−3.036	−1.838	−1.222

TABLE 9. Convergence of dimensionless resistance coefficient $F_3^{t_3}$ for a sphere moving perpendicular to a wall at various sphere-to-wall spacings. (*a*) Boundary collocation method, (*b*) weighted residual method

Substituting (B 1) into (2.15) and applying the no-slip boundary conditions on the surface of the body at discrete values of Z gives a system of linear algebraic equations which is independent of the θ-coordinate of the collocation points. Therefore only one-dimensional collocation is needed.

It is found that when the gap between the sphere and the wall is greater than half the radius of the sphere, the choice of collocation points is not critical if they are evenly spaced. When the sphere is located closer to the wall, some points are more important than others to achieve fast convergence. One important point is $Z = 0$ since it satisfies the no-slip boundary conditions on the ring covering the largest surface area on the particle and defines the maximum radius of the particle. The two end points $Z = \pm a$, the radius of the sphere, are also important. However, if collocation points are placed exactly at $Z = \pm a$, some of the coefficients of the matrix equation (2.15) become singular. One can either factor out the singularity or completely eliminate these terms by appropriate addition or subtraction of the linear algebraic equations as was done by Kim & Mifflin (1985) who encountered a similar situation in treating the problem of two spheres in an unbounded flow by the boundary collocation, truncated series solution technique. Alternatively, one can overcome the problem much more easily by simply replacing the two end points with two nearby points. The remaining collocation points are then evenly spaced along the circular arc.

Table 9(*a*) shows the results of convergence tests of the dimensionless force coefficient $F_3^{t_3}$ as a function of particle-to-wall spacing H/a for perpendicular motion using the boundary collocation method. $F_3^{t_3}$ is related to the hydrodynamic force by

$$F_3 = 6\pi\mu a U_3 F_3^{t_3}, \tag{B 2}$$

where U_3 is the velocity of the particle perpendicular to the wall. The numerical results are compared to the exact solution given by Brenner (1961). Convergence to at least three significant digits is obtained using eleven collocation points for gap widths as small as one-tenth of the sphere radius. When the gap width is larger than half the sphere radius only seven collocation points are needed to give four significant digit accuracy.

Table 9(*b*) shows the results of convergence tests of the dimensionless force coefficients $F_3^{t_3}$ for perpendicular motion using the weighted residual method. The convergence characteristics are surprisingly similar to those of the boundary collocation method shown in table 9(*a*). Because of the similarity of the convergence

	(a)				(b)			
$N\backslash H/a$	1.1276	1.5431	2.3524	3.7622	1.1276	1.5431	2.3524	3.7622
4	−2.016	−1.462	−1.283	−1.168	−0.1126	−0.0323	−0.00242	−0.000415
6	−2.116	−1.567	−1.308	−1.174	−0.0985	−0.0298	−0.00253	−0.000418
8	−2.144	−1.567	−1.308	−1.174	−0.0760	−0.0145	−0.00263	−0.000419
10	−2.152	—	—	—	−0.0723	−0.0146	−0.00264	−0.000422
12	−2.151	—	—	—	−0.0737	−0.0147	−0.00264	−0.000422
Exact	−2.151	−1.567	−1.308	−1.174	−0.0737	−0.0147	−0.00264	−0.000422

TABLE 10. Convergence of dimensionless resistance coefficients for a sphere moving parallel to a wall at various sphere-to-wall spacings. (a) F_1^t, (b) T_2^t

	(a)				(b)			
$N\backslash H/a$	1.1276	1.5431	2.3524	3.7622	1.1276	1.5431	2.3524	3.7622
4	−0.173	−0.0226	−0.00375	−0.00549	−1.334	−1.097	−1.023	−1.006
6	−0.149	−0.0202	−0.00351	−0.00553	−1.374	−1.100	−1.025	−1.006
8	−0.106	−0.0188	−0.00351	−0.00558	−1.382	−1.100	−1.025	−1.006
10	−0.0983	−0.0195	−0.00352	−0.00562	−1.388	−1.100	−1.025	—
12	−0.0983	−0.0195	−0.00352	−0.00562	−1.388	—	—	—
Exact	−0.0983	−0.0195	−0.00352	−0.00562	−1.388	−1.100	−1.025	−1.006

TABLE 11. Convergence of dimensionless resistance coefficients for a sphere rotating along a wall at various sphere-to-wall spacings. (a) F_1^r, (b) T_2^r

characteristics of both methods and the fact that the computation time using the weighted residual method is somewhat greater than that of the boundary collocation method, we shall only use the boundary collocation method in the computations which follow.

We now consider the non-axisymmetric motions, cases (2)–(4). For these motions we set

$$\left.\begin{aligned} f_1 &= \sum_{n=0}^{\infty} (A_n + B_n \cos 2\theta) P_n\left(\frac{Z}{a}\right), \\ f_2 &= \sum_{n=0}^{\infty} B_n \sin 2\theta P_n\left(\frac{Z}{a}\right), \\ f_3 &= \sum_{n=0}^{\infty} C_n \cos\theta P_n\left(\frac{Z}{a}\right), \end{aligned}\right\} \tag{B 3}$$

Again the system of linear algebraic equations is independent of the θ-coordinate of the collocation points, and only one-dimensional collocation is needed, even though the fluid motion is now three-dimensional. Moreover, for these cases, using the point $Z = 0$ produces a singular matrix even though for the axisymmetric case it did not. The problem is easily overcome by replacing the point $Z = 0$ by two closely spaced points $Z = \pm\epsilon$ as was done by Gluckman, Pfeffer & Weinbaum (1971). The remaining points are equally spaced along the circular arc as was done in the axisymmetric case.

Tables 10–12 show the results of convergence tests for the dimensionless force and torque coefficients as a function of particle-to-wall spacing. These coefficients are

	(*a*)				(*b*)			
$N\backslash H/a$	1.1276	1.5431	2.3524	3.7622	1.1276	1.5431	2.3524	3.7622
4	1.610	1.437	1.277	1.167	−0.9508	−0.9737	−0.9923	−0.9973
6	1.614	1.439	1.278	1.167	−0.9526	−0.9746	−0.9911	−0.9971
8	1.616	1.439	1.278	—	−0.9533	−0.9744	−0.9903	−0.9971
10	1.616	—	—	—	−0.9538	−0.9742	−0.9901	—
12	1.616	—	—	—	−0.9537	−0.9742	−0.9901	—
Exact	1.616	1.439	1.278	1.167	−0.9537	−0.9742	−0.9901	−0.9971

TABLE 12. Convergence of dimensionless resistance coefficients for a sphere rigidly held in a shear flow near a wall at various sphere-to-wall spacings. (*a*) F_1^s, (*b*) T_2^s

related to the hydrodynamic force and torque acting on the sphere as follows. For a sphere translating with velocity U_1 parallel to the wall, the force and torque exerted by the fluid on the sphere are given by

$$F_1 = 6\pi\mu a U_1 F_1^{t_1}, \quad T_2 = 8\pi\mu a^2 U_1 T_2^{t_1}. \tag{B 4a, b}$$

For a sphere rotating with angular velocity ω about the x_2 axis the force and torque exerted on the sphere is

$$F_1 = 6\pi\mu a^2 \omega F_1^r, \quad T_2 = 8\pi\mu a^3 \omega T_2^r, \tag{B 5a, b}$$

while for a shear flow with strength S past a rigidly held sphere the force and torque is

$$F_1 = 6\pi\mu a H S F_1^S, \quad T_2 = 4\pi\mu a^3 S T_2^S. \tag{B 6a, b}$$

Comparing with the exact solutions given by Goldman, Cox & Brenner (1967*a*, *b*), convergence to at least three significant digits is obtained for all coefficients for sphere-to-wall gap widths as small as only one tenth of the sphere radius using a maximum of twelve collocation points.

In order to check the convergence characteristics of the method for the general case when the particle is inclined at an arbitrary angle relative to the wall, the general double series representation of stokeslet strength (2.18) and general two-dimensional collocation over the body surface are required. Of course for the special case of a sphere, the drag and torque should be independent of the orientation angle. The degree to which the computed force and torque coefficients are independent of the orientation angle for a sphere serves as a further indication of the accuracy of the method.

Numerous convergence tests for the general two-dimensional collocation have been performed to find the number of collocation points in both the Z- and θ-directions needed to achieve convergence to a desired accuracy. The two-dimensional collocation points used in the following runs are arranged such that the rings, which are represented by constant values of Z, are evenly spaced along the spherical arc. At each ring the collocation points are evenly spaced along the θ-direction. The number of collocation points used at each ring is equal to the number of terms retained in the Fourier series representation of the density functions (2.18) while the number of rings used is equal to the number of terms retained in the Legendre series.

Tables 13 and 14 show numerical results of the dimensionless force and torque coefficients for a sphere with a fluid gap width of about one-half and one-tenth of the sphere radius respectively using the general two-dimensional collocation procedure.

α (degrees)	$F_1^{t_1}$	F_1^r	F_1^s	$F_3^{t_3}$	$T_2^{t_1}$	T_2^r	T_2^s
15	−1.566	−0.01955	1.439	−3.032	−0.01470	−1.100	−0.9742
30	−1.567	−0.01955	1.439	−3.032	−0.01470	−1.100	−0.9742
45	−1.567	−0.01957	1.439	−3.035	−0.01462	−1.100	−0.9742
60	−1.567	−0.01956	1.439	−3.037	−0.01467	−1.100	−0.9743
75	−1.567	−0.01950	1.439	−3.036	−0.01468	−1.100	−0.9742
Exact	−1.567	−0.01953	1.439	−3.036	−0.01465	−1.100	−0.9745

TABLE 13. Numerical tests of two-dimensional collocation for a sphere. $H/a = 1.5431$, α is the orientation angle of the sphere axis. 24 collocation points were used.

α (degrees)	$F_1^{t_1}$	F_1^r	F_1^s	$F_3^{t_3}$	$T_2^{t_1}$	T_2^r	T_2^s
				(*a*)			
15	−2.149	−0.09866	1.616	−8.91	−0.07467	−1.386	−0.9537
30	−2.150	−0.09886	1.616	−9.04	−0.07416	−1.387	−0.9537
45	−2.151	−0.09839	1.616	−9.24	−0.07408	−1.387	−0.9537
60	−2.151	−0.09815	1.616	−9.25	−0.07411	−1.387	−0.9537
75	−2.151	−0.09813	1.616	−9.26	−0.07412	−1.387	−0.9537
Exact	−2.151	−0.09829	1.616	−9.252	−0.07372	−1.387	−0.9537
				(*b*)			
15	−2.151	−0.09836	1.616	−9.23	−0.07352	−1.388	−0.9537
30	−2.150	−0.09838	1.616	−9.27	−0.07340	−1.387	−0.9537
45	−2.152	−0.09810	1.616	−9.26	−0.07387	−1.387	−0.9537
60	−2.151	−0.09859	1.616	−9.20	−0.07484	−1.387	−0.9537
75	−2.148	−0.1029	1.616	−9.31	−0.07605	−1.385	−0.9537
Exact	−2.151	−0.09829	1.616	−9.252	−0.07372	−1.387	−0.9537

TABLE 14. Numerical tests of two-dimensional collocation for a sphere at $H/a = 1.1276$. (*a*) Using 10 rings and 6 points at each ring. (*b*) Using 8 rings and 8 points at each ring

When the fluid gap width is one-half the sphere-radius the same arrangement of collocation points (given values of Z) and four points at each ring (given values of θ) are used for all orientation angles as shown in table 13. Comparing with the exact solution, the maximum error of all coefficients in any orientation is less than 0.5%. When the separation gap is only one-tenth of the sphere radius, two different arrangements of the collocation points are used as shown in tables 14(*a*) and 14(*b*). We find that although both sets of results exhibit good accuracy, the arrangement used in table 14(*a*) (ten rings and six points at each ring) is better than the arrangement used in table 14(*b*) (eight rings and eight points at each ring) when the orientation angle is larger than 45°, and vice versa when the orientation angle is smaller. This behaviour is to be expected since as $\alpha \to 90°$ fewer terms in the Fourier series, and thus fewer collocation points on each ring, are needed. In fact, as already demonstrated, in the limit of $\alpha = 90°$ only one term of the Fourier series and one-dimensional collocation in the Z-direction is required.

It should be noted that the coefficients on the left-hand side of the integral equations (2.15) depend only on the geometry and the form of the series representation of the stokeslet densities but not on the boundary conditions satisfied

	F^t_∞	
	Motion parallel to axis	Motion perpendicular to axis
	oblate	
a/b		
0.1	−0.8525	−0.6133
0.2	−0.8615	−0.6596
0.5	−0.9053	−0.7927
0.8	−0.9606	−0.9189
	prolate	
b/a		
0.8	−0.8404	−0.8788
0.5	−0.6020	−0.6895
0.2	−0.3570	−0.4742
0.1	−0.2647	−0.3812

TABLE 15. Force coefficients for a spheroid in an infinite fluid

on the particle surface or U_∞. Since the bulk of the computation time is used to evaluate the coefficient matrix for a given configuration, the force and torque coefficients may be determined in a single run for a given geometry at one instant in time using the two-dimensional collocation scheme for all four of the problems outlined at the beginning of this Appendix with a negligible increase in the computation time which would be required for a single problem. The computation time required for one configuration is approximately proportional to the square of the number of collocation points used and can be estimated by the formula $T = 0.0015N^2$, where T is the CPU time in minutes on an IBM 3081 computer and N is the total number of collocation points.

Appendix C

In this Appendix we list formulas for calculating the force and torque coefficients of a spheroid in an unbounded fluid. In the following a is the half-length, b is the radius and $\phi = a/b$ for both oblate and prolate spheroids. Tables 15 and 16 list some values of these coefficients.

When a spheroid is translating in an unbounded fluid it does not experience any torque. The drag coefficient for translatory motion is defined as

$$F^{t_1}_{1,\infty} = F_1/6\pi\mu c U_1, \tag{C 1}$$

where $c = b$ for an oblate spheroid and $c = a$ for a prolate spheroid.

The drag coefficient for translatory motion with arbitrary angle α toward the symmetry axis can be expressed as follows:

$$F^{t_1}_{1,\infty} = F^{t_1^*}_{1,\infty}\cos^2\alpha + F^{t_1^{**}}_{1,\infty}\sin^2\alpha, \tag{C 2}$$

where $F^{t_1^*}_{1,\infty}$ and $F^{t_1^{**}}_{1,\infty}$ represent the drag coefficients for translatory motion parallel and perpendicular to the axis of symmetry respectively. The coefficients $F^{t_1}_{1,\infty}$ and

	$T^{\tau}_{2,\infty}$		
	Flow parallel to axis	Flow perpendicular to axis	$T^{\tau}_{2,\infty}$
		oblate	
a/b			
0.1	−0.8525	−0.008525	−0.4305
0.2	−0.8615	−0.03446	−0.4480
0.5	−0.9053	−0.2263	−0.5658
0.8	−0.9606	−0.6148	−0.7877
		prolate	
b/a			
0.8	−0.8403	−1.313	−1.077
0.5	−0.6020	−2.408	−1.505
0.2	−0.3570	−8.924	−4.640
0.1	−0.2647	−26.47	−13.37

TABLE 16. Torque coefficients for a spheroid in an infinite fluid

$F^{t_1^{\bullet\bullet}}_{1,\infty}$ are given by Happel & Brenner (1973) and listed below for reference. For an oblate spheroid:

$$F^{t_1^{\bullet}}_{1,\infty} = -\frac{8}{3}\left\{\frac{2\phi}{1-\phi^2}+\frac{2(1-2\phi^2)}{(1-\phi^2)^{\frac{3}{2}}}\tan^{-1}\left[\frac{(1-\phi^2)^{\frac{1}{2}}}{\phi}\right]\right\}^{-1}, \tag{C 3}$$

$$F^{t_1^{\bullet\bullet}}_{1,\infty} = \frac{8}{3}\left\{\frac{\phi}{1-\phi^2}+\frac{2\phi^2-3}{(1-\phi^2)^{\frac{3}{2}}}\sin^{-1}(1-\phi^2)^{\frac{1}{2}}\right\}^{-1}, \tag{C 4}$$

For a prolate spheroid:

$$F^{t_1^{\bullet}}_{1,\infty} = \frac{8}{3}\left\{\frac{2\phi^2}{\phi^2-1}-\frac{(2\phi^2-1)\,\phi}{(\phi^2-1)^{\frac{3}{2}}}\ln\left[\frac{\phi+(\phi^2-1)^{\frac{1}{2}}}{\phi-(\phi^2-1)^{\frac{1}{2}}}\right]\right\}^{-1}, \tag{C 5}$$

$$F^{t_1^{\bullet\bullet}}_{1,\infty} = -\frac{8}{3}\left\{\frac{\phi^2}{\phi^2-1}+\frac{(2\phi^2-3)\,\phi}{(\phi^2-1)^{\frac{3}{2}}}\ln\left[\phi+(\phi^2-1)^{\frac{1}{2}}\right]\right\}^{-1}. \tag{C 6}$$

When a spheroid is rotating in an unbounded fluid it only experiences a torque. The torque coefficient is defined as

$$T^{\tau}_{2,\infty} = T_2/8\pi\mu b^2 c\omega. \tag{C 7}$$

The force experienced by a spheroid in an unbound shear flow is equal to that which it would have if it were translating in an otherwise unbounded quiescent fluid with a velocity equal to the incoming fluid velocity at the spheroid centre. The torque coefficient for a spheroid rigidly held in a shear flow at an arbitrary angle α is defined as

$$T^{S}_{2,\infty} = T_2/4\pi\mu b^2 cS. \tag{C 8}$$

This torque coefficient can be expressed as

$$T^{S}_{2,\infty} = T^{S^*}_{2,\infty}\cos^2\alpha + T^{S^{**}}_{2,\infty}\sin^2\alpha, \tag{C 9}$$

where $T^{S^*}_{2,\infty}$ and $T^{S^{**}}_{2,\infty}$ represent the coefficients for shear flow whose direction is parallel and perpendicular to the axis of symmetry of the spheroid, respectively. The

torque coefficients $T^{r}_{2,\infty}$, $T^{S^*}_{2,\infty}$ and $T^{S^{**}}_{2,\infty}$ have been obtained by Jeffery (1922) and listed below for reference. For an oblate spheroid:

$$T^{r}_{2,\infty} = -\frac{2}{3}\frac{1+\phi^2}{\gamma_1+\phi^2\gamma_2}, \tag{C 10}$$

$$T^{S^*}_{2,\infty} = -\frac{4}{3}\frac{1}{\gamma_1+\phi^2\gamma_2}, \tag{C 11}$$

$$T^{S^{**}}_{2,\infty} = -\frac{4}{3}\frac{\phi^2}{\gamma_1+\phi^2\gamma_2}, \tag{C 12}$$

while for a prolate spheroid:

$$T^{r}_{2,\infty} = -\frac{2}{3}\frac{1+\phi^2}{\phi(\gamma_1+\phi^2\gamma_2)}, \tag{C 13}$$

$$T^{S^*}_{2,\infty} = -\frac{4}{3}\frac{1}{\phi(\gamma_1+\phi^2\gamma_2)}, \tag{C 14}$$

$$T^{S^{**}}_{2,\infty} = -\frac{4}{3}\frac{\phi}{\gamma_1+\phi^2\gamma_2}, \tag{C 15}$$

where

$$\gamma_1 = \int_0^\infty \frac{\mathrm{d}\lambda}{(1+\lambda)\Delta}, \quad \gamma_2 = \int_0^\infty \frac{\mathrm{d}\lambda}{(\phi^2+\lambda)\Delta}, \quad \Delta = (\phi^2+\lambda)^{\frac{1}{2}}(1+\lambda). \tag{C 16a, b, c}$$

REFERENCES

Blake, J. R. 1971 A note on the image system for a stokeslet in a no-slip boundary. *Proc. Camb. Phil. Soc.* **70**, 303–310.

Brenner, H. 1961 The slow motion of a sphere through a viscous fluid towards a plane surface. *Chem. Engng Sci.* **16**, 242–251.

Brenner, H. 1964 The Stokes resistance of an arbitrary particle – II. An extension. *Chem. Engng Sci.* **19**, 599–629.

Brenner, H. & Gaydos, L. J. 1977 The constrained Brownian movement of spherical particles in cylindrical pores of comparable radius. Models of the diffusive and convective transport of solute molecules in membranes and porous media. *J. Colloid Interface Sci.* **58**, 312–356.

Chen, T. C. & Skalak, R. 1970 Stokes flow in a cylindrical tube containing a line of spheroidal particles. *Appl. Sci. Res.* **22**, 403–441.

Dabros, T. 1985 A singularity method for calculating hydrodynamic forces and particle velocities in low-Reynolds-number flows. *J. Fluid Mech.* **156**, 1–21.

Fung, Y. C. 1981 *Biomechanics: Mechanical Properties of Living Tissues*. Springer.

Gluckman, M. J., Pfeffer, R. & Weinbaum, S. 1971 A new technique for treating multiparticle slow viscous flow: axisymmetric flow past spheres and spheroids. *J. Fluid Mech.* **50**, 705–740.

Goldman, A. J., Cox, R. G. & Brenner, H. 1967*a* Slow viscous motion of a sphere parallel to a plane wall. I. Motion through a quiescent fluid. *Chem. Engng Sci.* **22**, 637–651.

Goldman, A. J., Cox, R. G. & Brenner, H. 1967*b* Slow viscous motion of a sphere parallel to a plane wall. II. Couette flow. *Chem. Engng Sci.* **22**, 653–660.

Goren, L. & O'Neill, M. E. 1980 Asymmetric creeping motion of an open torus. *J. Fluid Mech.* **101**, 97–110.

Happel, J. & Brenner, H. 1973 *Low Reynolds Number Hydrodynamics*, 2nd rev. edn. Noordhoff.

Hsu, R. 1985 Hydrodynamic interaction of an arbitrary particle with a planar-wall at low Reynolds number. Ph.D. dissertation, City University of New York.

JEFFERY, G. B. 1922 The motion of ellipsoidal particles immersed in a viscous fluid. *Proc. R. Soc. Lond.* A **102**, 161–179.

KIM, S. & MIFFLIN, R. T. 1985 The resistance and mobility functions of two equal spheres in low-Reynolds-number flow. *Phys. Fluids* **28**, 2033–2045.

KUCABA-PIETAL, A. 1986 Nonaxisymmetric Stokes flow past a torus in the presence of a wall. *Arch. Mech.* **38**, 647–663.

LADYZHENSKAYA, O. A. 1963 *The Mathematical Theory of Viscous Incompressible Flow.* Gordon & Breach.

LEAL, L. G. & LEE, S. H. 1982*a* Particle motion near a deformable fluid interface. *Adv. Colloid Interface Sci.* **17**, 61–81.

LEE, S. H. & LEAL, L. H. 1982*b* The motion of a sphere in the presence of a deformable interface. II. A numerical study of the translation of a sphere normal to an interface. *J. Colloid Interface Sci.* **87**, 81–106.

LEICHTBERG, S., WEINBAUM, S. & PFEFFER, R. 1976 A theory for the coaxial slow viscous motion of finite clusters of spheres in unbounded Poiseuille flow and its application to rouleaux formation. *Biorheol.* **13**, 165–179.

LEWELLEN, P. 1982 Hydrodynamic analysis of microporous mass transport. Ph.D. dissertation, University of Wisconsin-Madison.

LIGHTFOOT, E. N. 1974 *Transport Phenomena and Living Systems.* Wiley.

LIRON, N. 1978 Fluid transport by cilia between parallel plates. *J. Fluid Mech.* **86**, 705–726.

LIRON, N. & MOCHON, S. 1976 The discrete-cilia approach to propulsion of ciliated micro-organisms. *J. Fluid Mech.* **75**, 593–607.

ODQVIST, F. K. G. 1930 Uber die Randwertaufgaben der Hydrodynamik Zaher Flussigkeiten. *Math. Z.* **32**, 329–375.

RALLISON, J. M. & ACRIVOS, A. 1978 A numerical study of the deformation and burst of a viscous drop in an extensional flow. *J. Fluid Mech.* **89**, 191–200.

SKALAK, R., CHEN, P. H. & CHIEN, S. 1972 Effect of hematocrit and rouleaux on apparent viscosity in capillaries. *Biorheol.* **9**, 67–89.

TOZEREN, H. 1984 Boundary integral equation method for some Stokes problems. *Intl J. Num. Meth. Fluids* **4**, 159–170.

WAKIYA, S. 1959 Effect of a submerged object on a slow viscous flow (Report V). Spheroid at an arbitrary angle of attack. *Res. Rep. Fac. Engng Niigata Univ. Japan* **8**, 17–30 (in Japanese).

WANG, H. & SKALAK, R. 1969 Viscous flow in a cylindrical tube containing a line of spherical particles. *J. Fluid Mech.* **38**, 75–96.

YOUNGREN, G. K. & ACRIVOS, A. 1975 Stokes flow past a particle of arbitrary shape: a numerical method of solution. *J. Fluid Mech.* **69**, 377–403 (and corrigendum **69**, 813).

YUAN, F. & WU, W. Y. 1987 The Stokes flow of an arbitrary prolate axisymmetric body towards an infinite plane wall. *Appl. Math. Mech. SUT, Shanghai, China*, **8**, 17–30.